Parts, Tuule Mall; Ferrantelli, Andrea; Naar, Hendrik; Thalfeldt, Martin; Kurnitski, Jarek

Wax actuator's empirical model development and application to underfloor heating control with varying complexity of controller modelling detail

Published in:
Journal of Building Performance Simulation

DOI:
10.1080/19401493.2023.2201818

Published: 01/01/2023

Document Version
Peer-reviewed accepted author manuscript, also known as Final accepted manuscript or Post-print

Please cite the original version:
Parts, T. M., Ferrantelli, A., Naar, H., Thalfeldt, M., & Kurnitski, J. (2023). Wax actuator's empirical model development and application to underfloor heating control with varying complexity of controller modelling detail. *Journal of Building Performance Simulation*, *16*(6), 772-796. https://doi.org/10.1080/19401493.2023.2201818

Note: Snapshot PDF is the proof copy of corrections marked in EditGenie, the layout would be different from typeset PDF and EditGenie editing view.

Author Queries & Comments:

Q1 : Please note that the ORCID has been created from information provided through CATS. Please correct if this is inaccurate.

Response: I have added ORCID for all authors in the CATS system. For some reason these do not show here.

Q2 : Please check if the affiliations of all the authors and Physical address of the corresponding author included are appropriate.

Response: The affiliation b should be written out as "Nearly Zero Energy Buildings Research Group" as in physical address

Q3 : Please edit the abstract down to no more than 1s50 words.

Response: Resolved

Q4 : Please note that the Funding section has been created by information given in the acknowledgements and from CATS xml, and the "acknowledgements" section has been removed. Please correct if this is inaccurate.

Response: Resolved

Q5 : The funding information provided (Estonian Ministry of Education and Research and European Regional Fund; H2020 project Finest Twins) has been checked against the Open Funder Registry and we failed to find a match. Please check and resupply the funding details.

Response: The project link at European Commission is here: https://cordis.europa.eu/project/id/856602

Q6 : The disclosure statement has been inserted. Please correct if this is inaccurate.

Response: Resolved. Is correct.

Q7 : The reference "Akaike 1974" is listed in the references list but is not cited in the text. Please either cite the reference or remove it from the references list.

Response: Resolved

Q8 : Please provide missing city for the reference "[b20]" references list entry.

Response: Resolved

CM1 : Please replace the gmail address with tuule.parts@taltech.ee for corresponding author contact

CM2 : In column Description, the "delayed heating signal", "On" and "Off" should not be highlighted in yellow. Please remove the highlight or take the table from the clean version of the submitted article.

CM3 : Please remove unnecessary and confusing grey background from February week in the last column

CM4 : In the 2nd row, column Parameters, the [47] should be a reference to Kull, Thalfeldt, Kurnitski 2020. Remove it from here, added to the footnote. Increase Step and Parameter colum widths so that the table takes up the whole page width.

CM5 : The appendix title has gone lost before the Table C1. It should be - "C. Model fitting results for the characteristic times". Also the table should fit on one page.

CM6 : The article has been written in American (US) English. The system has made changes to change it to British English in the conclusion and some other parts (z->s and o ->ou). However, not everywhere. The Figures are in American English so please change back to American English.

CM7 : please fit into one column width

CM8 : Replace with correction from attachment (Figure4).

CM9 : Please replace with better sized new version from attachment (Figure18).

Wax actuator's empirical model development and application to underfloor heating control with varying complexity of controller modelling detail

Tuule Mall Parts[a,b], Andrea Ferrantelli[a,b,d], Hendrik Naar[c], Martin Thalfeldt[a,b], Jarek Kurnitski[a,b,d]

[a] FinEst Centre for Smart Cities (Finest Centre), Tallinn University of Technology, Tallinn, Estonia

[b] nZEB Research Group, Tallinn University of Technology, Tallinn, Estonia

[c] Mechanics and Fluids and Structures Research Group, Tallinn University of Technology, Tallinn, Estonia

[d] Department of Civil Engineering, Aalto University, Aalto, Finland[Q2]

CONTACT Tuule Mall Parts tuulemall@gmail.com Nearly Zero Energy Buildings Research Group~~FinEst Centre for Smart Cities (Finest Centre)~~, Tallinn University of Technology, Ehitajate tee 5, Tallinn 19086, Estonia

History : received : 2022-5-20 accepted : 2023-4-3

ABSTRACT

This paper investigates how a simulated room's energy and temperature performance are affected if its underfloor heating control is modelled with increasing detail. Experiments were performed to develop and calibrate an empirical model of wax motor and to calibrate the valve curve. These models were used to implement and test the On/Off and proportional-~~–~~integral (PI) control processes at various levels of modelling detail. Controllers were implemented by gradually adding optimized control parameters, signal delay, calibrated valve curve, signal modulation, and actuator modelling. The On/Off control dead band and PI parameters exhibited the largest impact, reducing energy use (1%–5%) and temperature fluctuations (ca 1 K). Modulating the PI output signal increased temperature fluctuations to the same amplitude as On/Off with 0.5 K dead band, increasing space heating demand by 1.3%. The wax actuator counted for less than 1%; however, it increased time delays to maximally 7 min and remarkably changed the mass flows[Q3].

KEYWORDS

- Phase change material
- hydronic underfloor heating
- temperature control
- detailed control modelling
- control valve characteristic
- grid interaction

FUNDING

This study[Q4] was supported by the European Regional Development Fund via the Estonian Centre of Excellence in Zero Energy and Resource Efficient Smart Buildings and Districts ZEBE, grant 2014-2020.4.01.15-0016, from the Estonian Research Council through the grants PSG409, PRG658, and DigiAudit, from the Estonian Ministry of Education and Research and European Regional Fund (grant 2014-2020.4.01.20-0289), and by the European Commission through the [Q5]H2020 project Finest Twins (grant No. 856602).

1. Introduction

Buildings[Q1] are responsible for 36% of greenhouse gas emissions and for about 40% of the total energy consumption, of which 1/3 goes into heating (Bienvenido-Huertas et al. 2021). Extensive involvement of renewables in the energy production is important for reducing carbon emissions (Rogelj 2018), but it poses serious problems to the electricity grid, due to the highly fluctuating nature of photovoltaic and wind generated energy. To guarantee stability and efficiency of the distribution network in the imminent future, matching electricity demand and renewable energy generation needs to be realized rather swiftly (Boßmann and Staffell 2015).

Electricity-based heating systems, such as heat pumps together with hydronic underfloor heating (UFH), are increasingly used in residential buildings to reduce heating demand. These provide both electrification of the heating demand as well as structural thermal storage. Balancing the power grid of high shares of renewable energy is thus possible, to some extent, through demand-side management (Wolisz et al. 2020; Zhang, Good, and Mancarella 2019). Dynamic control of these systems exploits indeed the buildings' intrinsic structural thermal mass to shift both heating and cooling timing, without reducing the indoor climate quality (Wolisz et al. 2020; Le Dréau and Heiselberg 2016; Pedersen, Hedegaard, and Petersen 2017; Reynders, Diriken, and Saelens 2017). Importantly though, the thermal fluctuations in the enclosure critically affect the charging and discharging of some fraction of this thermal mass. An accurate balance of the power grid via structural thermal storage should thus be accomplished through several control methods (Zhang, Good, and Mancarella 2019; Wolisz et al. 2016, 2020).

One way to participate in the balancing of the power grid is bidding on the so-called manual Frequency Restoration Reserve, which helps stabilizing the electricity grid by restoring the required frequency of the grid. Open for public participation is in most countries the manual Frequency Restoration Reserve, which is provided by the Transmission System Operator. This is a tertiary control reserve, which steps in to correct longer lasting deviations that cannot be fixed by the other upstream balancing services alone (Okur, Heijnen, and Lukszo 2021). At least 1 MW is often required for bidding (Okur, Heijnen, and Lukszo 2021), but intermediators aggregating several heat pumps could provide enough power (Zhang, Good, and Mancarella 2019). In such Frequency Restoration Reserve market, the providers must be able to switch their loads within 5 to 15 min (Artelys 2017; Fingrid Oyj 2022). To this aim, heat pumps require manual intervention and overwritten control (Lindahl 2020); the start-up time of the heat pump system could also generate a bottleneck that is critical to the local system response to the grid. Even if the heat pump can be activated as fast as within 5 min, a heat sink is needed for its energy to avoid overheating the small amount of water in the heat pump's closed circuit. This would lead to stopping the electricity consumption and not fulfilling the bid. In case of inverter-based heat pump systems, large storage tanks are typically not installed, and the building structures should be used as a heat sink. This requires opened valves in the hydronic heating system, e.g. UFH manifold. However, valves in UFH systems are controlled by thermoelectric actuators with solid wax, which react relatively slowly. In closed valve positions, the system volume is very small and temperature limits in the heat pump circuit may be reached too quickly when the heat pump is started at full power. A slow movement of the actuator's piston with slow opening of the valves would then hinder the aggregator from delivering the bidden load for the grid.

To ensure energy flexibility and thermal comfort simultaneously in real applications, the control algorithms need to be carefully designed, tested, and validated. For initial development and testing, building performance simulations (BPS) are a suitable tool for speeding up the testing for different heating systems, building types, climates, usage profiles. Simulations are also needed to compare different algorithms at exact same boundary conditions. However, BPS are well known to simplify the control process to close-to-ideal, ignoring control parameter tuning, signal time delays, actual valve characteristic, and actuators. Usually, modelling of these is omitted as the control time constant is several orders of magnitude smaller than that of the whole system. The room temperature measurement time delay could be as large as 2 min (Burt and de Podesta 2020). Additionally, a delay of 2–3 min for the actuator-valve mechanism is normally assumed (Danfoss A/S 2017; Ventilation Control Products Sweden AB 2022). Even together, these timescales are too small to significantly alter the annual energy consumption of the building, especially if the users adapt the setpoint in response to temperature fluctuations induced by the delay. This timescale could still be important in simulations aimed at testing control algorithms that include logic for bidding or experimental situations for analysing the valve effects on volume flows.

Modelling the control in a detailed manner requires, among other details, a wax motor model. This is a major contribution of the present study, since an implementation that allows investigating the above systems' control with sufficient accuracy is still missing. Additional applications of PCMs into the buildings' design are currently implemented into BPS with a broad scope, from, e.g. thermally activated wall panels (Klimeš, Charvát, and Ostrý 2019) to PCM tanks (Li et al. 2020). These have often been modelled as thermal hysteresis (Goia, Chaudhary, and Fantucci 2018). Sometimes, the actuators are simply modelled as a delay in BPS (Wetter 2009), or more commonly also as hysteresis, modelling their movement (Rizzello, Naso, and Seelecke 2019). To our knowledge, there can be found only one detailed wax actuator model for HVAC applications, namely a physical enthalpy-based model in IDA ICE (EQUA AB 2020), which was tested in Kull, Thalfeldt, and Kurnitski (2021). The study calibrated the physical wax motor model by numerically optimizing the parameters and compared the calibrated model error to a simple characteristic model. The calibration and comparison were performed only on a short and periodic signal. It was concluded that the parameters of the simple model should be variable, to perform well also in other situations. In this constant case the characteristic model induces slightly smaller errors than the physical model. The main limitation of the physical model lies however in the extensive amount of material testing or optimization required to determine all the properties of each wax motor product in practice.

Overall, scientific publications on the experimental as well as the modelling aspect of wax actuators are indeed very scarce. The effect of wax motors on BPSs has not been shown in the literature. In this study, we attempt at filling this compelling research gap that is entailed from the above discussion by developing a characteristic model with variable parameters and testing its effect on simulation results in a realistic control process. Motivation is given by both formal advancements and possible effects of the modelling on energy performance predictions, control algorithm testing and power grid balancing.

More into detail, several research questions emerge:

1 How can we characterize HVAC wax actuators with limited material testing? This study proposes a new empirical wax actuator model (with discrete hysteresis) for simulations in IDA ICE.
2 How much time does the valve opening with wax motors take? Can it be managed within 5 min, so that it would match the limit imposed by the frequency market for energy grids?
3 In the modelling of UFH for testing temperature control algorithms, the control is often assumed to be continuous (e.g. PI). However, the actual control is often On/Off (modulated) and exhibits a wax motor delay. How much are temperature control accuracy and energy performance then affected?
4 How do wax motor and modulation effects compare to performance differences from other modelling simplifications such as non-optimal control parameters, no delays in signals and linear valve characteristic?

To address these problematics, in this study we first performed experiments on wax motors to develop and calibrate an empirical model of wax actuator. Then, measurements were performed to estimate the valve performance in one UFH circuit and calibrate the valve curve. The wax actuator and the valve curve models were then used in BPS to implement and test the various levels of detail in modelling the control algorithms.

The paper is organized as follows. In Section 2, we provide a short overview of wax actuators and their modelling. Section 3 explains our methodology, featuring wax motor model development, valve curve estimation, and setup of room simulations. Section 4 fully reports experimental and simulation results, including a discussion at each stage. Finally, we draw our conclusions in Section 5, and include some additional experimental inputs and results in the Appendix.

2. **Wax actuators**

Thermoelectric wax actuators are electrically controlled and use paraffin wax as phase change material (PCM) for volume change(Burt and de Podesta 2020; Danfoss A/S 2017). The wax is solid at room temperature and liquid at higher temperatures. It is heated by a positive temperature coefficient (PTC) heater. These actuators are known by other names as well, such as wax motors (used in this work, abbreviated as WM), wax pellet actuators, thermo-electric actuators, or thermal actuators (Ventilation Control Products Sweden AB 2022; Klimeš, Charvát, and Ostrý 2019; Li et al. 2020; Goia, Chaudhary, and Fantucci 2018). In the absence of an electric heating signal, the system actuator-valve is normally closed. When voltage is applied, the wax starts melting and expanding, thus moving the valve's piston. By the action of a system of springs, the piston movement reduces the actuator's inner height, thus opening the valve. Such method of valve control has been used in UFH for a long time, as the actuators are silent and durable(Wetter 2009). Slower reactions also avoid the water hammer that is associated with motorized valves. Additionally, wax actuators are used before fan coils in cooling systems, and for pressure-independent control valves in heating systems. Radiator thermostats also include similar motors; however, these are often based on the expansion of liquid or gas instead of the phase change of the wax.

Some wax actuators use a continuous control with voltage between 0 and 10 V. Others use discrete control with a binary heating input, namely no voltage for no heating and 230 V or 24 V for heating. Continuous 0–10 V wax actuators still use 24 V to power the PTC heater. Therefore, if a controller with continuous output such as a PI controller is used to control the UFH wax actuators, the continuous signal must be modulated into a binary signal for the PTC heater.

The 0–10 V actuators can theoretically stay partially open. However, the partial opening control is easier for valves that have a logarithmic valve characteristic curve, i.e. a logarithmic volume flow dependency on the valve opening. In UFH manifolds, quick-opening valves are instead applied. These exhibit most of the change in volume flow when the valve is only slightly open. The partial flow would be realized only in a very small range of valve opening; therefore, these valves perform close to On/Off with either actuator, by using continuous or discrete control. Simpler 24-V On/Off-motors are often applied, which is the case of this work.

The actuator's cross section, valve, and part of the manifold are shown in Figure 1. The piston movement in function of the wax temperature change is shown in Figure 2. The hysteresis of up and down movements is generated by the temperature difference at the movement start and stop on both ends, caused by thermal inertia of the wax and friction of the internal parts that include a spring (Vernatherm 2023). The hysteresis in temperature can be linearized for simplification and presented on a time scale that is dependent on the binary heating signal, as shown in Figure 3. This linearized simple model was called 'characteristic model' in Kull, Thalfeldt, and Kurnitski (2021). Of course, the opening and closing process can be non-linear according to Figure 2. In the context of this paper, the different time periods in Figure 3 are called 'characteristic times' and defined as follows:

- Dead time (t_{dead}): solid wax heating up to the melting temperature, no volume change.
- Rise time (t_{rise}): phase change of the wax from solid to liquid and expansion.
- Hold time (t_{hold}): liquid wax cooling down to the melting temperature, no volume change.
- Fall time (t_{fall}): phase change of the wax from liquid to solid and compression.

Figure 1. Valve opening with wax actuator warming visualized with part of manifold, figure parts adapted from (Beijing MUYY Technologies Co., Ltd 2023) and (The Underfloor Heating Site 2023).

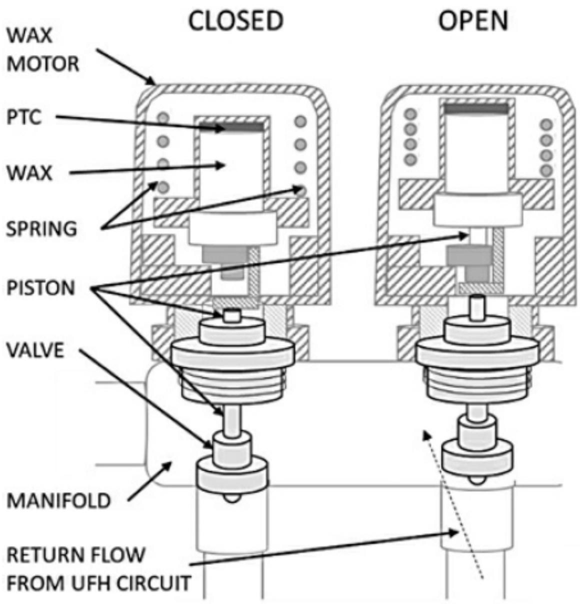

Figure 2. Theoretical piston movement (displacement) according to wax temperature, adapted from (Vernatherm 2023).

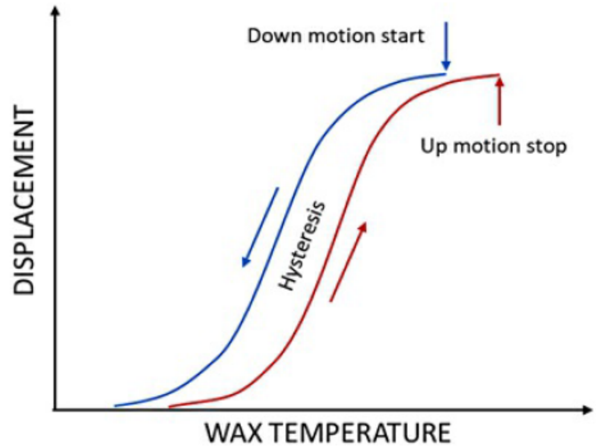

Figure 3. Definition of characteristic times for the normalized linear displacement of the piston of wax actuator or valve.

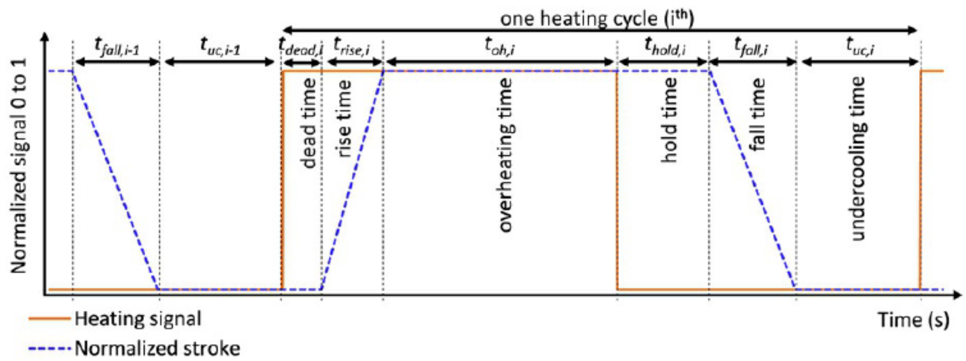

Based on these, additional times for analysis could be calculated as well:

- Full activation time (FAT): $t_{FAT} = t_{dead} + t_{rise}$
- Deactivation time (DAT): $t_{DAT} = t_{hold} + t_{fall}$
- Overheating time (t_{oh}): the time when the valve is fully open, but the motor is still heated, liquid wax is heated up
- Undercooling time (t_{uc}): the time when the motor is not heated, and the valve is fully closed, solid wax is cooling down

The characteristic times could be empirically estimated and do not need physical modelling of the wax temperature and phase change process to make the wax actuator model. This would make the method more approachable than estimating all physical parameters such as material properties, mass, volume, conductivities, spring properties, etc. In Kull, Thalfeldt, and Kurnitski(2021), the characteristic times were constant. In this work, the models are fitted for each characteristic time depending on previous actions. The following assumptions can be drawn:

- The dead time should be dependent on how low the temperature of solid wax has fallen, represented by the undercooling time:

$$t_{\text{dead},i} = a_{\text{dead}} \cdot e^{-\frac{t_{uc,i-1}}{\tau_{\text{dead}}}} + b_{\text{dead}}$$

  where $t_{\text{dead},i}$ [s] is the dead time at cycle i, which depends on the undercooling time of the previous cycle $t_{uc,i-1}$ [s] and on the empirically fitted parameters a_{dead} [s], τ_{dead} [s], and b_{dead} [s], where τ represents the time constant, a and b are the linear regression parameters.
- The hold time should be dependent on how high the temperature of liquid wax has risen, represented by the overheating time (with similar definitions):

$$t_{\text{hold},i} = a_{\text{hold}} \cdot \left(1 - e^{-\frac{t_{oh,i}}{\tau_{\text{hold}}}}\right) + b_{\text{hold}}$$

- The rise and fall times should be constant for a given wax motor product and at constant ambient temperature, as the wax amount is constant and therefore so is the amount of energy given with the heating signal through PTC during melting, or the heat loss during solidification.

3. Methods

A visualization of the general workflow of the study is depicted in Figure 4. The model of wax motor and the valve curve achieved from measurements were used to estimate their effect in simulations. The *displacement*, the linear movement or position of the piston dependent on the given electric signal, was measured without the valve being connected to the UFH system, see Figure 5. The displacement measurements were used to define the empirical model of the wax actuator. Then, we installed the wax motor on a valve in the UFH manifold and measured the volume flow while knowing the electric signal, see Figure 1. The wax motor model from previous step was then used to calculate the piston's linear displacement in flow measurements. The valve opening to volume flow characteristic curve – the valve curve – could be calibrated from these measurements and calculations. The resulting models were used to assess the effect of the wax actuator in BPS.

Figure 4. General overview of the research process.

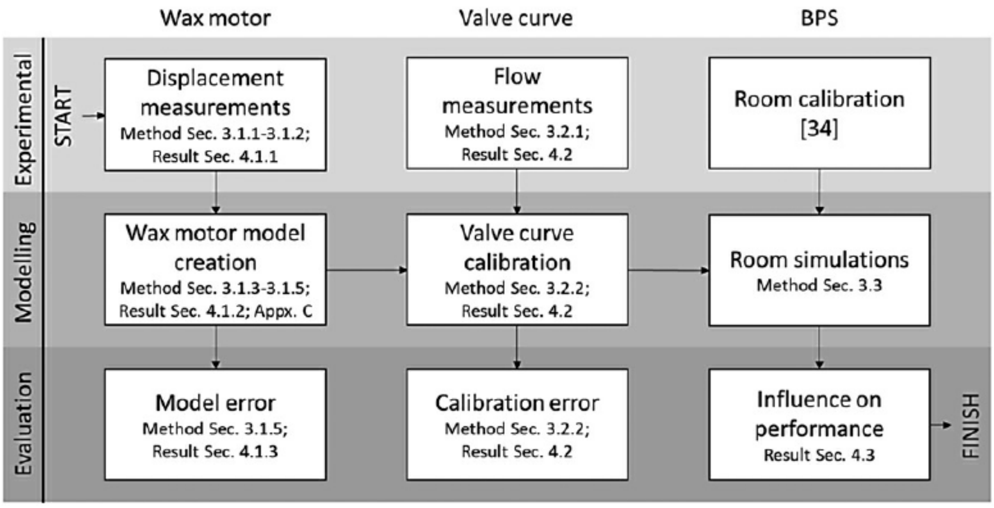

Figure 5. Visualization of a wax actuator functioning and measurements when not installed in the manifold (HBM Finland 2022), in measurement the system was vertical (90 degrees turned).

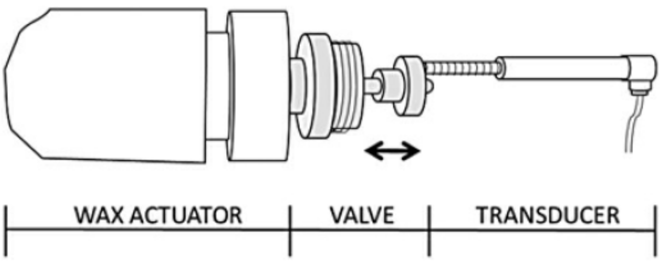

We have divided the experiments into (i) displacement measurements of the actuator but not in the UFH system, and (ii) flow measurements within the system, for two main reasons. First, a separate wax motor model would enable applying any valve model on top of the wax motor model. As valve characteristics are quite well known and modelled, this would result in a broader field of application, possibly with no further measurements. Secondly, it was not possible to directly measure the wax motor position in the same experiment as flow measurements, since measuring the piston displacement inside the manifold's pipes or through transparent piping during execution is not commonly available.

The main physical difference between the two experiments was the existence of water flow. In the flow measurement case, there was water flow against the piston, driven by circulation pump. In the displacement measurement case, there was none. Still, we assumed that this water flow had insignificant influence on the movement of the piston, thus we used the wax motor model generated from the displacement measurement case on the flow measurement case without modifications. This assumption was supported by a comparison of pressures. The pump in the small measured system generated maximally a 30 kPa pressure head in the example volumetric flow measurements. The wax motor, on the other hand, generates 1000 kPa while expanding. If we assume a 1 cm^2 valve head cross section, the force is ca 100 N. This was confirmed by some data sheets where the force was claimed to be, i.e. 100 N ± 5%(Lindab 2021). Therefore, the force that is generated on the valve by the pump (3 N) was over 30 times lower than the force applied by the wax motor (100 N). The piston movement would not be affected significantly by the pressure difference that is generated by the circulation pump.

3.1. Wax motor model development

3.1.1. Measured actuators

The wax actuators that were measured in this work were commercial products that are commonly installed in the UFH manifolds in Estonian buildings. Products A and B, originating from separate producers, were tested. For product B, four different exemplars were tested just to see whether products and exemplars were different. Describing the whole potential range of variance was out of the scope of this work, so no more products nor exemplars were included. In the data sheet of product A, the positioning time t_{FAT} is claimed to be 3 min, the full movement range (also called 'nominal stroke') is 2.5 mm, and the positioning force is 105 N. The data sheet of product B does not include these details.

In some measurements, a quick-opening valve was screwed to the actuator as shown in Figure 5. In such case, the initial position of the spring in the motor is slightly more compressed, therefore the full movement range could be smaller. However, the movement time should be similar as it depends on the time of wax phase change at constant power. This is the effect that was analysed. As a result, the combinations are named A, Av, B1, B1v, B2, B2v, B3v and B4v, where numbers label the exemplars, and 'v' stands for the quick-opening valve if attached. The explanation of all measured combinations is shown in the first four columns of Table 1. The last column is explained in the next section (3.1.2.~~0~~).

Table 1. Measured wax actuator and valve combinations for clarification of combination names; in the last column are the measured heating profiles.

Combination	Product	Exemplar No.	Valve included	Heating profiles measured (signal on–off)
A1	A	1	no	15 min–15 min~~; 15 min–45 min; 5 min–5 min~~
				15 min–45 min
				5 min–5 min
A1v	A	1	yes	15 min–15 min
B1	B	1	no	15 min–15 min~~; 15 min–45 min; 30 min–30 min; 10 min–10 min; 18 min–6 min; 3 min–3 min~~
				15 min–45 min;
				30 min–30 min
				10 min–10 min
				18 min–6 min
				3 min–3 min
B1v	B	1	yes	15 min–15 min
B2	B	2	no	15 min–15 min
B2v	B	2	yes	15 min–15 min~~; 15 min–45 min~~
				15 min–45 min
B3v	B	3	yes	15 min–15 min
B4v	B	4	yes	15 min–15 min~~; 15 min–45 min; random 5 to 15 min~~
				15 min–45 min
				random 5 to 15 min

Table 2. Empirical wax motor model with its calculation process.

Symbol		Unit/range	Description	Logic expression in IDA ICE
IN	s	0/1	Heating signal	Input
Empirical model of wax actuator: calculation process	s_D	0/1	Delayed heating signal	s lagged by 5 sec
	k_s	[-1,1]	Signal slope	s-s_D, hold for 4 sec
	t_{ls1}	s	Last On-time	Integrate s, reset when $k_s > 0.5$
	t_{ls0}	s	Last Off-time	Integrate 1-s, reset when $k_s < -0.5$
	$t_{uc,i-1}$	s	Last undercooling time	Integrate 1-s when not($t_{DAT} > t_{ls0}$ & s_D ==0), reset when $k_s < -0.5$, $t_{uc,i-1}$=0 until t_{DAT} available
	$t_{dead,i}$	s	Dead time	$-192\ (3) \cdot \exp\left(-t_{uc,i-1}/780\right) + 219\ (13) \pm 13$
	$t_{rise,i}$	s	Rise time	$-30(3) \cdot \exp\left(-t_{uc,i-1}/1140\right) + 142(22) \pm 21$
	$t_{oh,i}$	s	Overheating time	Integrate s when not($t_{FAT} > t_{ls1}$ & d==1), reset when $k_s > 0.5$, $t_{oh,i}$=0 until t_{FAT} available
	$t_{hold,i}$	s	Hold time	$\begin{cases} 195\ (6) \cdot \left(1 - \exp\left(-\frac{t_{oh,i}}{240}\right)\right) + 30\ (5), \text{for product A} \\ 82\ (3) \cdot \left(1 - \exp\left(-\frac{t_{oh,i}}{600}\right)\right) + 58\ (2), \text{for product B} \end{cases}$
	$t_{fall,i}$	s	Fall time	$\begin{cases} 180, \text{for product A} \\ 123, \text{for product B} \end{cases}$
	$t_{FAT,i}$	s	Full activation time	$t_{dead,i} + t_{rise,i}$
	$t_{DAT,i}$	s	De-activation time	$t_{hold,i} + t_{fall,i}$
	c_{dead}	0/1	Is this currently dead time?	$t_{dead,i} > t_{ls1}$ & s_D ==1
	c_{rise}	0/1	Is this currently rise time?	$t_{FAT,i} > t_{ls1}$ & s_D ==1 & not c_{dead}
	c_{fall}	0/1	Is this currently fall time?	$t_{DAT,i} > t_{ls0}$ & s_D ==0 & not c_{hold}
	k_{rise}	1/s	Rise ramp	Integrate $1/t_{rise}$ when c_{rise}, reset every 3 min, [0, 1]
	k_{fall}	1/s	Fall ramp	Integrate $1/t_{fall}$ when c_{fall}, reset every 3 min, [0, 1]
	c_{hold}	0/1	Is this currently hold time?	$t_{hold,i} > t_{ls0}$ & s_D ==0
OUTPUT	h	[0,1]	Wax motor (+ valve piston's) normalized linear movement, limited between 0 and 1	If c_{dead}: h=0 Else if c_{rise}: h=k_{rise} Else if c_{hold}: h=1 Else if c_{fall}: h=k_{fall} Else: h= s_D

Table 3. Main building parameters.

Parameter	Value and unit	Comment
Floor area	100 m^2/10.4 m^2	House/room

Room window area	2 × 3 m^2	south and west
Windows ~~Total~~ U-value ~~of windows~~	0.75 W/m^{2}K	total
Glazing g-value ~~of glazing~~	0.3	
External walls U-value ~~of external walls~~	0.12 W/m^{2}K	timber-frame
Floor U-value ~~of floor above outdoor air~~	0.08 W/m^{2}K	concrete, above outdoor air
Avg. ~~T~~ thermal bridges ~~(average)~~	0.031 W/K/m^2	area of external surface
Infiltration at Δp 50 Pa ~~pressure difference~~	0.6 m^3/h/m^2	area of external surface
Fixed infiltration flow	0.0048 L/s/m^2	area of external surface
Internal walls	Adiabatic	
UFH PEX piping ~~(Wet installation)~~	20 × 2.0 mm	300 mm intervals, wet install
Floor cover upon piping	40 mm of screed	no cover on top
UFH power ~~nominal heat output~~	68 W/m^2	nominal heat output
Design temperatures	34/29°C	heating curve in App~~endix~~. B
Over-dimensioning	40%	

Table 4. Implementation of all control scenarios for both On/Off (Thermostat) and PI control.

Step	Parameters	PI (P_)	On/Off (O_)
0 (business-as-usual)	T_{Db}=2K K=0.3 t_i=300s t_t=30s	T_{room}, T_{set} → PI → $\dot{V}_{auth}$	T_{room}, T_{set} → On/Off → $\dot{V}_{auth}$
CP (adapted parameters)	T_{Db} =0.5K CP [47]: K=18 t_i=2300s t_t=30s	T_{room}, T_{set} → PI / CP → $\dot{V}_{auth}$	T_{room}, T_{set} → On/Off / CP → $\dot{V}_{auth}$
D (added delay)	Added delay t_D=2 min	T_{room}, T_{set} → D → PI / CP → $\dot{V}_{auth}$	T_{room}, T_{set} → D → On/Off / CP → $\dot{V}_{auth}$
VC (calibrated valve curve)	Sections 3.2 and 4.2	T_{room}, T_{set} → D → PI / CP → VC → $\dot{V}_{auth}$	T_{room}, T_{set} → D → On/Off / CP → VC → $\dot{V}_{auth}$
MC (control signal modulation)	Figure 8 and Figure 19	T_{room}, T_{set} → D → PI / CP → MC → VC → $\dot{V}_{auth}$	Not applicable
WM (added wax motor)	Table 2	T_{room}, T_{set} → D → PI / CP → MC → WM → VC → $\dot{V}_{auth}$	T_{room}, T_{set} → D → On/Off / CP → WM → VC → $\dot{V}_{auth}$

An initial controller (On/Off or PI) is always included, the other components/parameters are gradually added or adapted. T_{Db} is the dead band, K is the proportional gain, t_i is the integration time, t_t is the tracking time, and t_D is the time delay. Adapted PI parameters taken from Kull, Thalfeldt, Kurnitski (2020).

Table 5. Temperature fluctuation and energy consumption results for all cases; air temperature setpoint deviations dT are from 21°C and energy consumption results Q_h are in kWh/m^2/week.

	Temperature fluctuations				Energy consumption			
	January week		February week		January week		February week	
ID	dT	MAE(T)	dT	MAE(T)	Q_h	$\Delta Q_{h,w}\%$	Q_h	$\Delta Q_{h,w}\%$
O_0	0.49	0.597	0.33	1.092	2.55	5.71%	2.42	4.84%
O_CP	0.05	0.195	-0.03	0.682	2.42	0.36%	2.32	0.41%
O_D	0.05	0.2	-0.03	0.691	2.41	-0.12%	2.32	0.25%
O_VC	0.05	0.2	-0.03	0.69	2.41	-0.12%	2.32	0.21%
O_WM	0.06	0.215	0	0.628	2.41	0.00%	2.31	0.00%
P_0	-0.03	0.128	-0.08	0.637	2.41	0.08%	2.28	0.68%
P_CP	-0.09	0.033	-0.13	0.447	2.37	-1.63%	2.20	-2.75%
P_D	-0.09	0.038	-0.13	0.453	2.37	-1.67%	2.20	-2.71%
P_VC	-0.1	0.044	-0.14	0.462	2.37	-1.67%	2.21	-2.54%
P_MC	-0.07	0.149	-0.11	0.589	2.40	-0.48%	2.24	-0.80%
P_WM	-0.05	0.150	-0.08	0.676	2.41	0.00%	2.26	0.00%

~~Greyed out values single out irrelevant combinations for BPS.~~

3.1.2. Displacement measurements

We measured the displacement of the wax actuator and valve combination's last element as shown in Figure 5. The sensor was a vertically fixed displacement transducer with 10-mm measuring range. Additionally, the actuator's surface temperature, the room temperature and the actuator's supply voltage were measured. The measurement step was 1 s and the data was logged by an HBM CX22BW data recorder (HBK 2022) through a MX840A measuring bridge (HBK 2021).

In all experiments, the actuators were powered and controlled by a Siemens LOGO! 24CE controller with 24-V transistor outputs (Siemens 2021), which generated the heating profiles as shown in the last column of Table 1. The first value before the dash is the heating time during which the wax actuator is heated, with the 24 V signal given as input. The second number after the dash is the cool-down time in between two heating cycles. Therefore, a '15min-45min' profile means that the voltage was 24 V for 15 min, then turned off for 45 min. This was repeated periodically and the test duration for each profile is given in Appendix A.

The heating profiles were chosen to ensure complete opening and closing of the valve during each heating cycle. If this did not happen, the tested heating profile was excluded from this study, since those cycles where the valve is not fully opened or closed are typically not used for 24-V actuators. Based on literature and initial tests, at least 3–5 min of heating and cooling time was needed. In this study, the cut-off limit for this exclusion remained close to 3 min for both heat-up and cool-down. Longer gaps between heating charges were tested, for allowing the wax to cool down between cycles and to analyse its effect on valve opening time. A 15 min–15 min heating profile was measured for all combinations to enable comparison, and most heating profiles were tested on the motor B1.

3.1.3. Post-processing and cut-off conditions

The measured displacement was normalized for each experiment. The maximum displacement is the closed cold position when the head was at the lowest position. When the valve opened, the head moved higher, and the measured values were lower. The difference between the fully open and fully closed positions, the stroke, was identified in each experiment for normalizing the displacement as follows:

$$\mathrm{normDisplacement} = \frac{|\mathrm{displacement} - \mathrm{stroke}|}{\mathrm{stroke}}$$

where $\mathrm{displacement}$ [mm] is the measured time series during one experiment. The 0-V or 24-V input voltage was also normalized to a time series with values between 0 and 1, the heating signal.

For each heating cycle in each experiment, we estimated the characteristic times described in Section 2. For an ideal trapezoid displacement as shown in Figure 3, all these times are clearly defined. However, for continuous smooth response, the cut-off between these periods is not clear. In this work, the rise and fall times were separated from the rest by defining a minimum slope of the ramping. We assumed that the linear change from 0 to 1 would take no longer than 10 min in total. For a normalized stroke, this is 10% in a minute, so a slope steeper than 0.83% in 5 s was classified to be part of the rise time. To smoothen out measurement errors, an average slope for 5 seconds was used instead of a 1-second measurement step. For fall classification, the slope was steeper and therefore a twice as large limit of −1.67% change in 5 s was used. These limits were chosen by qualitatively assessing that the classified periods did not have discontinuities (example result in Section 4.1.2, Figure 10). When the stroke should have been 0, a slack of 5% was applied to exclude small shift offsets. The timesteps that were not included into rise or fall times were separated into dead time, hold time, overheating time, and undercooling time according to heating signal and normalized displacement values, according to the logic described in Section 2. The input heating signal was accounted to be 1 when larger than 0.5, or 0 when equal to 0.5 or lower.

3.1.4. Models of characteristic times

The four characteristic times – dead time, rise time, hold time, and fall time – were identified for each heating cycle, and a regression model for calculating each characteristic time could be defined by fitting the experimental data. The models for all non-constant characteristic times in Section 2 can be given as

$$t_{\mathrm{out}} = a \square f(t_{\mathrm{in}}/\tau) + b$$

where t_{in} is t_{uc} in Equation (1) and t_{oh} in Equation (2), and t_{out} is t_{dead} or t_{hold} correspondingly. The parameters τ, a and b are empirical parameters and need to be fitted. To find the parameters and to test these assumptions, τ was first estimated. The correlation between $f(t_{\mathrm{in}}/\tau)$ and the output time t_{out} was calculated for different τ values, and the τ value with best correlation was chosen. The assumed models from Equations (1) and (2) were then tested by using linear models (lm) and the parameter significance was tested according to p-values in R (R Core Team 2020). If the p-value for any parameter was larger than .001, no significance was found and the model was not used. If significant, the parameters a and b were fitted.

The parameters in characteristic times' models can change for each product, due to a different wax mass and build of the motor. If no common model was significant, we applied multi-level models (lme) in R, which vary the parameter b for the product models. However, common models are clearly to be preferred. Although the rise time was assumed to be constant, it can be seen in the results (Section 4.1.2) that it was not. A similar model as in Equation (1) was therefore applied.

The entire fitting process was based on the results from Sections 4.1.1 and 4.1.2, and is described into detail in Appendix C. The resulting models are shown in Table 2 with yellow background. These models were compiled into one as the next section describes.

3.1.5. Empirical model of wax motor

The entire process from displacement measurements to empirical model is shown in Figure 6. The final empirical linear-segments model of a wax motor was a combination of the four characteristic time models – dead time, rise time, hold time, and fall time – each with product-specific parameter values. For implementation, the characteristic time lengths need to be calculated into displacement at any given time. This concluding implementation is shown in Table 2 as a calculation process from the heating signal to the linear movement of the wax motor valve. Figure 3 helps with the visualization of the different time periods and notation. Based on the heating signal *s(t)* and the same signal delay – *d(t)*, jumps in the signal were determined as its slope $k_s(t)$. Based on the heating signal and its slope, the last 'On' and 'Off' times of the heating signal were calculated. The undercooling time was found in one heating cycle, when both the normalized displacement and the heating signal were zero. Then, it was used in the obtained formulas to estimate the dead time and rise time for the next cycle.

Figure 6. The process of estimating the empirical wax motor model from the displacement measurements.

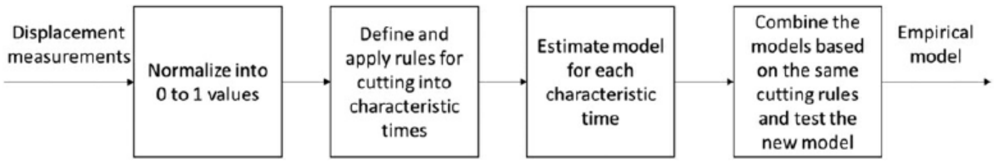

When the normalized displacement rose to 1 or its gradient slowed down, the overheating time started and was registered until the heating signal dropped to 0. The following hold time was calculated according to this overheating time. The fall time was a constant for a given wax motor product. After the normalized displacement had reached 0, the undercooling time started again. The final normalized displacement value was set to 0 during dead time and to 1 during the hold time. During rise time and fall time the value should be ramping up or down. Therefore, the ramping speed was calculated and integrated from the start of the given period, to get the output displacement.

The obtained models were then tested on the measured data. For each experiment, both the mean absolute error (MAE) and root mean square error (RMSE) were evaluated, andthese were compared between motors and profiles. The linear segments model for one of the products was implemented and tested in IDA ICE. Product B was chosen as it was installed by design in the test facility discussed in the next section.

3.2. Valve curve estimation

3.2.1. Volume flow measurements

To simulate the effect of modelling the control details on BPS, the characteristic curve of the valve was needed. Instead of using a theoretical curve, an actual curve was estimated from measurements (see Section 3.2.2). For the measurements inside the UFH system, the wax actuator B2 was installed in the UFH manifold of the TUT nZEB test facility. This is a 100-m^2 house that was constructed for testing nZEB solutions. It features balanced heat recovery ventilation, a ground source, and an air-to-water heat pump system with both radiators and UFH, among other technologies. The building model has been previously built and calibrated in the IDA ICE software, as detailed in Kull, Thalfeldt, and Kurnitski (2019a). The floor plan of the test facility is shown in Figure 7 and the key parameters for modelling the building are listed in Table 3.

Figure 7. Floor plan of the test facility, experiment room R6 marked in red.

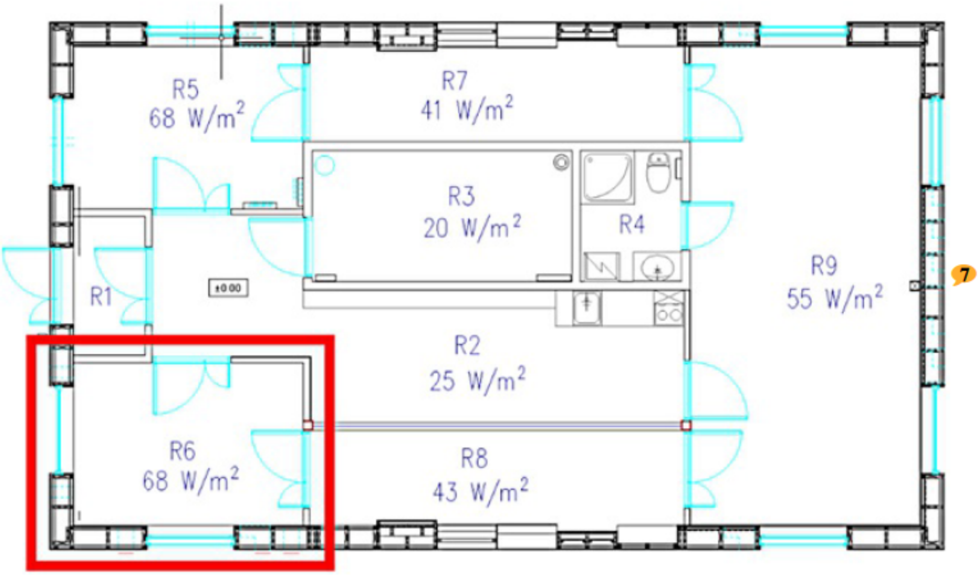

The aim was to calculate the given valve's characteristic curve for further modelling as a proof of concept, so only one motor was measured. In the experiment, the LOGO controller (see Section 3.1.1) generated 15 min–15 min heating profiles – 15 min-long heating signals, with a 15-min gap between heating cycles. The volume flow was generated by significant setpoint changes in one UFH circuit that serves a 10-m^2 room, marked with a red box in Figure 7, which was controlled as described in Section 3.3. The volume flow was measured by the heat metre Sensus Pollustat E (Sensus Inc. 2021). All other circuits were closed due to much lower setpoints. The measurements are fully described in Maivel, Ferrantelli, and Kurnitski (2018; Võsa, Ferrantelli, and Kurnitski 2019; Kull, Thalfeldt, and Kurnitski 2019b).

3.2.2. Valve curve and authority correction

The measured volume flows and the heating signal were used to estimate the valve characteristic curve for the given UFH circuit. First, the empirical model developed according to Sections 3.1.4 and 3.1.1 was applied to estimate the linear valve displacement due to the electrical heating signal from the controller. The *characteristic valve curve* is the relationship between this displacement and the measured volume flow.

To apply a valve curve for simulations, a model is needed for mapping volume flow to any valve displacement. The measured valve curve develops in two parts. First, the linear valve opening creates open area which in ideal case would be linearly correlated to volume flow. However, this theoretical valve curve is changed by valve authority, which describes how well the valve can control the volume flow.

The valve curve model was estimated in two steps: first we defined the theoretical quick opening valve curve, which is typical of UFH valves, then the valve authority effect. All the parameters were chosen such that the final volume flow best fits the measurements.

The *quick opening valve curve* is where most of the volume flow increase happens at low opening values. There are no precise values defined, so the theoretical normalized valve curve, here relation h to $\dot{V}$ was here defined in a simplified way with three points (Kumar 2017),

- The minimum efficient displacement (h_0) – the normalized displacement from which the volume flow starts to increase
- The maximum efficient displacement (h_{max}) – the normalized displacement starting from which the volume flow does not increase further
- The mid-point (h_p, $\dot{V}_p$) – the point from which quick opening stops and slower opening continues

where h is the normalized shift from 0 to 1, and $\dot{V}$ is the normalized volumetric flow. The valve authority can significantly change the theoretical valve curve. To take this into account, the theoretical curve $\dot{V}$ was modified by the valve authority N into normalized and authority-corrected volume flows ($\dot{V}_{auth}$) (Johnson Controls LTD 2020) with

$$\dot{V}_{\text{auth}} = \sqrt{\frac{\frac{1}{N}}{\frac{1}{N} - 1 + \frac{1}{\dot{V}^2}}}$$

where $\dot{V}$ is the theoretical valve curve and N is the valve authority. The valve authority can be calculated from the following formula (Petitjean 1994),

$$N = \frac{dp_v}{dp_{\text{pump}}} = \frac{dp_{\text{pump}} - dp_{\text{sys}}}{dp_{\text{pump}}}$$

where dp_v, dp_{pump}, dp_{sys} are the pressure differences across the control valve in kPa, the pump, or the rest of the system with a fully open valve. dp_{sys} can be estimated by adding up pressure drops across each component in the system. In our tested configuration, we estimated that the system consists of both the circuit's straight components (1.1 kPa) and the bends in its pipe (7.1 kPa), a heat metre (4.5 kPa), a balancing valve on the main pipe (10.8 kPa), and balancing valves on each circuit's supply side (3.6 kPa). Altogether, dp_{sys} results in 27.1 kPa. The pump works at second speed and generates 30 kPa, therefore dp_v results in 2.9 kPa.

As the theoretical curve consists of linear segments, the Evolutionary Microsoft Excel Solver was applied to minimize the MAE between the measured and calculated $\dot{V}_{\text{auth}}$ numerically. The parameters h_0, h_p and $\dot{V}_p$ were varied to find the optimum. The limits were set as 0.1 to 0.3 for h_0, 0.1 to 1 for h_p, and 0 to 1 for $\dot{V}_p$. The h_0 was forced to be lower than h_p. The parameter $h_{\max}$ was set to 1 and the part where the valve opening was above 0.95 or below 0.05 was excluded from the error calculation, since although carrying many points, the flow variation was very small.

3.3. Room control simulations

To quantify the influence of the wax actuator and other control modelling details on energy performance and temperature control accuracy, several control scenarios were defined in the IDA ICE building simulation model. The modelled building and room were described in Section 3.2.1. The UFH in the room was modelled with an 'HCFloor model', which is basically a floor layer with different temperature (CEN 2008). The layer temperature develops with heat transfer from the piping to the layer material calculated according to logarithmic temperature differences. The supply temperature and volume flow of the liquid were given as inputs, the pressure and return temperature were modelled. The heating curve is included in Appendix B.

The installed power and schedules of internal gains defined by the Estonian legislation for energy performance calculations (Majandus-ja taristuminister 2015) were used, with an average internal heat gain of 4 W/m². The flow rate of the balanced heat recovery ventilation was 0.5 l/s/m². The supply air temperature was 18°C and the ventilation was constantly working. The Estonian Test Reference Year climate data for Tallinn (Kalamees and Kurnitski 2006) were applied. The first week in January and the second week in February were chosen to be simulated, as these have similar heating consumption but different solar heat gains. The heating consumption was 2.4 kWh/m²/week with IDA ICE default PI control. The solar heat gains were 0.15 kWh/m²/week and 0.82 kWh/m²/week in the January and February weeks respectively. The average dry bulb outdoor temperatures were −1.9°C in January and −6.8°C in February. A longer period was not simulated, as the empirical wax motor model currently requires timesteps of 5 s, which dramatically increases both simulation time and output files size.

The On/Off thermostat (O) and PI controller (P) cases were simulated for enabling comparisons, and both included a gradual increase in the level of detail. First, the business-as-usual simulations were defined, with IDA ICE default parameters that are typical for BPS simulations, corresponding to IDs O_0 and P_0. Then, step-by-step adapted control parameters, signal delay, adapted valve curve, signal modulation, and wax motor model were added. The process listing the sequential steps that correspond to the simulated scenarios is depicted in Table 4. On top of business-as-usual cases, first, the default control parameters (CP) were adapted in step CP. These are dead band (Db) for the On/Off controller and proportional gain K, integration time Ti and tracking time Tt for the PI controller. A 2-min delay (D) of input signal from the room temperature sensor to the controller, which is usually not considered (Wen and Smith 2001), was added starting from step D in cases O_D and P_D (Elnaklah, Walker, and Natarajan 2021). The calibrated authority-corrected quick-opening valve curve (VC) was then included. It was estimated as described in Section 3.2.2 and implemented in IDA ICE with small linear segments replacing the IDA ICE default linear control. Modulation of the continuous PI control signal, the modulation control (MC) was then applied in step MC on PI only as the On/Off output is already binary. Since the given 24 V wax actuators can only be controlled by a binary signal, the continuous output of the PI controller was translated with an hourly modulation, where at the beginning of each hour the algorithm decided whether and for how long to heat. The applied modulation control principle is shown in Figure 8. Finally, the developed empirical wax actuator model of product B was finally included in the cases O_WM and P_WM (where 'WM' stands again for 'wax motor').

Figure 8. Implementation of the modulation for the PI output into wax motor's input, the heating signal s. The calculation is performed once per hour.

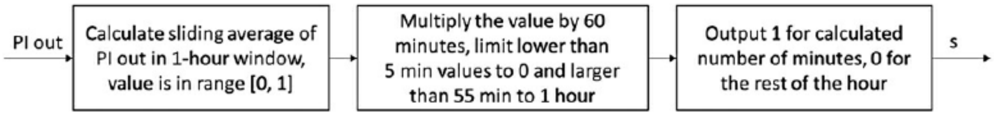

The most detailed cases O_WM and P_WM were used as the benchmark for all scenarios of the same controller. The comparison of energy consumption between different cases is sensible only at similar comfort levels, since lower temperatures would clearly result in lower energy consumption for heating. All simulations were thus initially carried out with a constant air temperature setpoint, which was then shifted iteratively until the operative temperature at 0.6 m from the floor in the middle of the room was below 21°C for up to approximately 33 h per week. This corresponds to the 20% limit for weekly deviation from the indoor climate class boundaries (EN 16798-2:2019 standard (CEN 2019)). Finally, the temperature fluctuations and heating energy consumption of the scenarios were compared.

3. Results and discussion

4.1. Wax motor modelling

4.1.1. Displacement measurements

The displacement is the linear movement of the actuator's piston triggered by electric signal, and its measurements described in Section 3.1 were used to define the empirical model of the wax actuator. Some examples of the displacement during a 15 min–15 min heating profile for each of the measured actuators are shown in Figure 9. There was a clear difference between the first period (left) and the following periods (visualized on top of each other on the right), as the motors were not conditioned identically before the beginning of each experiment. The figure shows that the wax in motor B1 was already warmed up before the first cycle. There has been a slight movement in the measuring device during the first cycle for B2. However, the first period conditions the motors and we can see that the following periods performed very similarly within each motor's measurements. There was almost no difference for cases with and without valve for the same motor either. Larger differences were found between different products, and small differences existed among instances of the same product. In the observed cases, the response for motor A1 looked like a trapezoid, while the product B motors had a slight movement even during the overheating. Quite likely, these differences could be caused by different general builds, covers, materials, etc. The product A's datasheet states that the cover is made of polycarbonate, this is not known for product B but the diameter of the motor B cover is 15% smaller. The actuator heights are very similar. The smooth change in displacement for product B makes it challenging to separate the rise time and overheating time, which is why the limits for ramps were defined as in Section 3.1.3.

Figure 9. Different wax motors' normalized displacement dynamics in the 15 min–15 min profile as shown by the heating signal (normalized voltage).

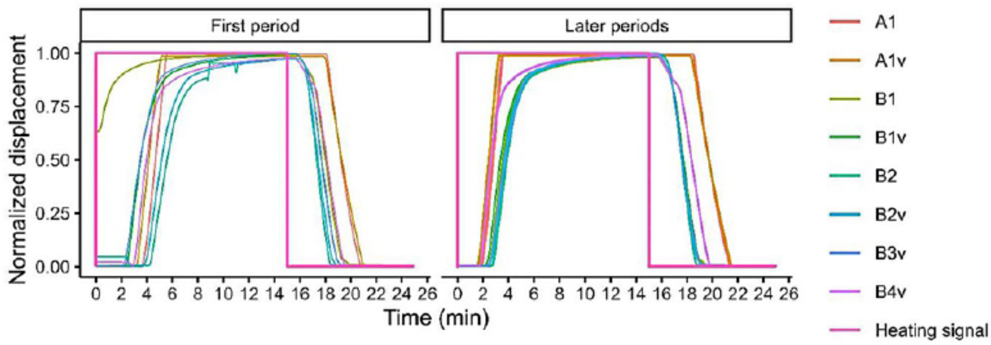

4.1.2. Cut-offs for characteristic times

The characteristic times of a wax motor – dead time, rise time, hold time, and fall time – were defined in Section 2 and summarized in Figure 3. Their estimation relied on the definition of the cut-off conditions for the periods. A sample result of the cut-off conditions is shown for a 15 min–15 min period of motor B3v in Figure 10. After filtering out some cases where the estimation failed as one or more of the characteristic times were estimated to be zero, 380 periods remained to be analysed. All resulting characteristic times are shown in Figure 11, where they are coloured according to the motor. The rise and fall times varied less than the dead and hold times. This was expected, as these should be constant for one product at the same room temperature. However, while the fall time shows to be mostly constant for one motor, the rise time has a more than 1-min variance for product B.

Figure 10. Example of how the characteristic times have been separated with cut-off definitions. The black line indicates the heating signal.

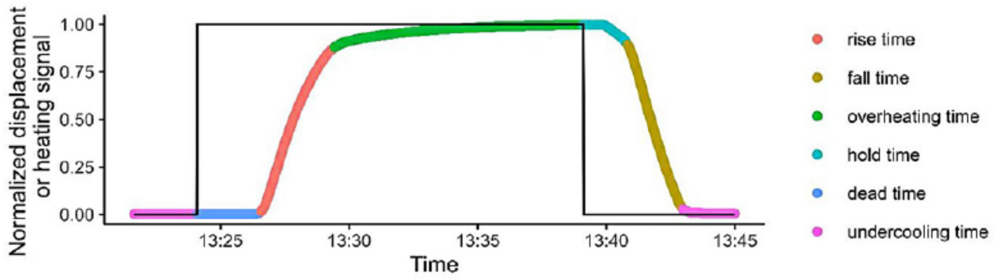

Figure 11. Characteristic times identified from all experiments, motor with and without valve grouped together.

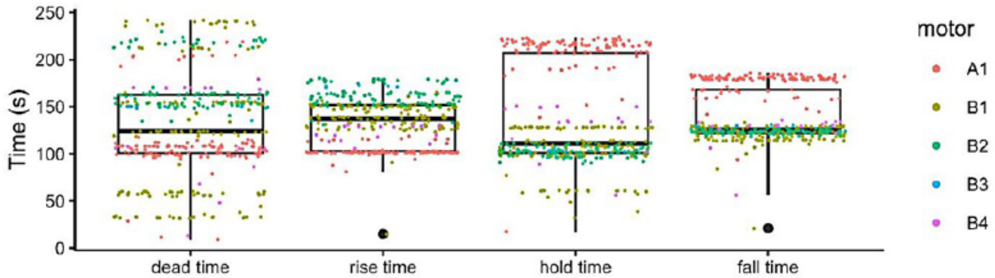

For heat pump inclusion in grid balancing, it is also important that the valves would open within 5 min. The full activation time t_{FAT} was calculated by adding up the dead and rise times. In most cases, the t_{FAT} was very close to 5 min, as shown in Figure 12. However, there were some cycles when t_{FAT} exceeded 5 min, yet staying below 7 min. For product B, these were of experiments where the cool-down time was 30 min or 45 min, and the wax could cool down more. The limit was exceeded also for the first period of 10 min–10 min and first three periods of 15 min–15 min profiles, due to the previous longer cool-down. For product A, even the 15 min–45 min profile's cycles were very close to the limit. However, falling to either side of the limit depended heavily on the definition of allowed ramp definitions. These influenced the cut-off between rise time and overheating time. For reaching below 5 min for all profiles, standby heating could be activated. The control would need to keep the wax at higher than room temperature with short heating pulses, which do not open the valve. The suitable pattern for standby heating should be determined either by experiments or with a physical model, which can handle profiles with short heating times.

Figure 12. FAT dependence on preceding undercooling time and motor's producer. The points are measured values, the lines show modelled values, the shaded area the modelling errors; the dashed line indicates the 5-min limit.

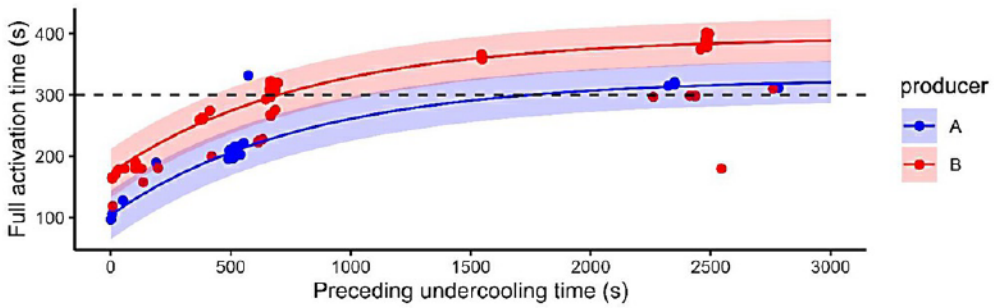

4.1.3. Empirical model performance

The mean absolute errors between measured and modelled displacement for some profile-motor combinations are shown in Figure 13. On the left, the examples from motor B1 show that there was a tendency for lower error in longer profiles, where undercooling and overheating dominate in the period. At these times the displacement is the easiest to model, as it is almost constant and close to 0 or close to 1. Therefore, the error is also the smallest, reducing the average error. The graph on the right illustrates the differences between experiments with and without the valve. No clear conclusion can be drawn from the slight differences. Results for motor A were more precise and there were slight differences between different samples of the same B motor. All the fitting errors are shown in Appendix A, Table A1. For all the profiles, the MAE remained below 10% (0.1) and the RMSE below 15% (0.15); the average MAE is 0.041 or about 4%. Examples of the typical, the best, and the worst performance for one hour are shown in Figure 14. The graph for A1 shows the suitable shape choice for the empirical model. For motor B, the heat-up process differed, but the effective volume flow corrected the slight difference, as shown in the next section. In the worst case, the maximum delay between the measured and simulated signal start was 1 to 1.5 min.

Figure 13. Error estimations for all measured profiles of one motor (left) and for all combinations of one profile (right).

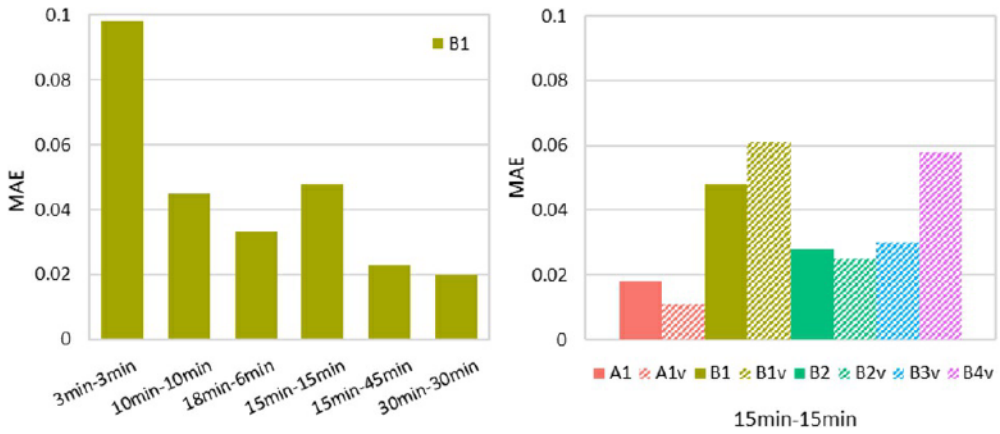

Figure 14. Performance of estimated wax motor model on predicting normalized displacement.

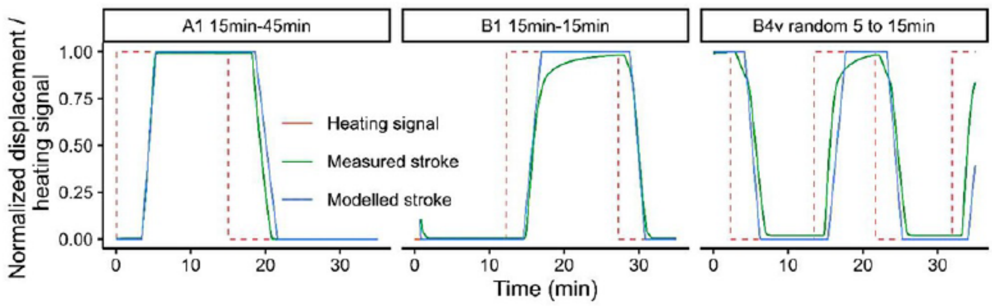

4.2. Volume flow modelling

We recall that the volume flow model, i.e. the characteristic curve of the valve, was needed to estimate the effect of modelling the volume flow in detail on BPS (Section 3.2). An example of the measured volume flows during one heating cycle that was measured in the test facility is given in Figure 15. Additionally, the input heating signal, with empirical model calculated valve displacement, and the modelled volume flow are shown. The modelled volume flow was obtained by fitting the theoretical model from Section 3.2.2. The graph of measured and modelled volume flow to displacement is shown in Figure 16, on the left, with estimated valve curves as follows: the theoretical valve curve is shown with dashed line, and the authority-corrected valve curve with solid line. The authority-corrected valve curve matched the measurements the best when the three-point quick opening characteristics were at h_p = 0.41, $\dot{V}_p$ = 0.5, $h_{\min}$ = 0.17. For the considered region, the MAE was 1.02%. In the graph on the right, the error between the measured and modelled authority-corrected valve curves is shown.

Figure 15. Measured (solid) versus modelled (dashed) volumetric flows, plus heating input signal (red) to the wax motor.

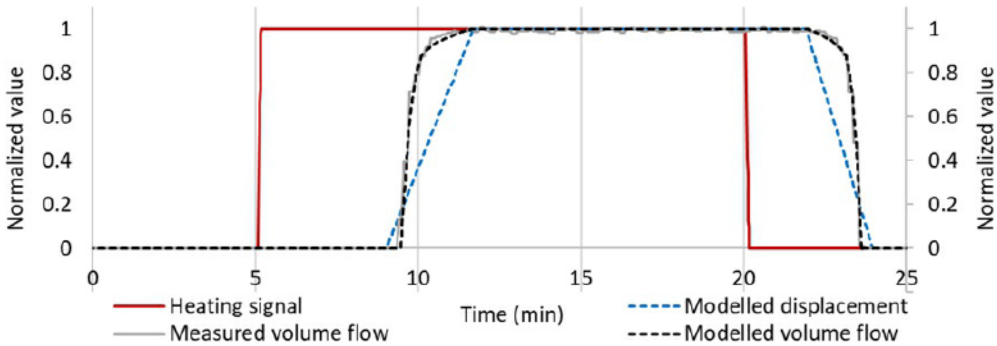

Figure 16. Valve curve modelling process and result on the left; measured versus modelled volume flows on the right.

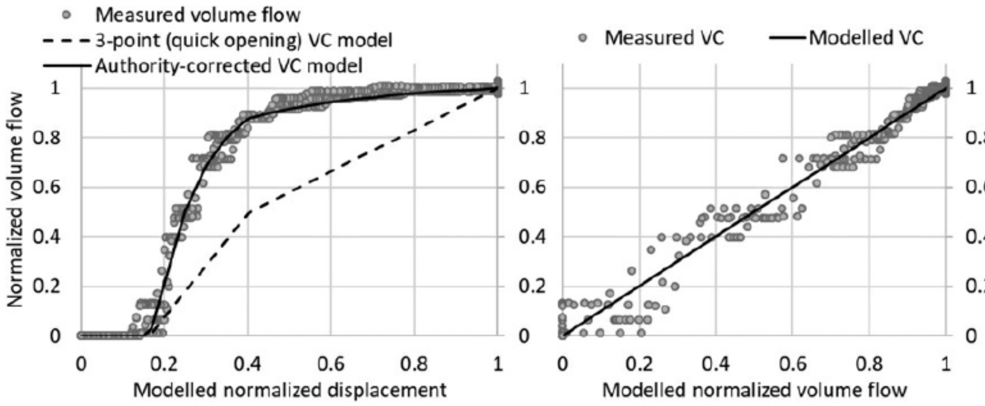

4.3. Effect on energy performance simulations

In section 3.3, several control scenarios were defined in IDA ICE to quantify the influence of the wax actuator and other elements of control process on energy performance and temperature control accuracy. In this section, we compare the results of the energy performance simulations. We recall that the '0' case was the business-as usual case, namely a simulation model with close-to-ideal control of the UFH system. This ignores the modelling of both wax motors (WM) and exact valve curves VC, while the PI control or On/Off thermostats were represented by parameters that are set to default values commonly used for BPS. The other scenarios use adapted control parameters CP, then sequentially add time delay D to the input signal, a VC; modulation control (MC), and finally, a WM. The level of modelling detail is therefore gradually increased from ideal to WM.

For comparability of energy consumption, air temperature setpoints were shifted so that 20% of the operative temperature remained below 21°C (Section 3.3). The applied setpoint shifts for all the cases, and the resulting energy consumption is shown in Table 5. In the columns, the air temperature shift from 21°C *dT* and the MAE of the air temperature MAE(*T*) characterize the temperature fluctuations. Q_h is the floor heating energy consumption per square metre of floor area per observed week, and its relative difference was calculated as $\Delta Q_h = (Q_h - Q_{h,w})/Q_{h,w}$ [%] for the given week. This quantified the consumption under-/ overestimation in the observed case, compared to the most detailed case O_WM or P_WM, respectively.

The table shows that only adding the wax motor onto the previous level of detail does not change the energy consumption a lot. There are larger changes in one step, such as correcting the parameters or adding modulation. However, the whole process of adding modelling detail, changes the results vividly both in temperature fluctuations and in energy consumption. The changes are discussed in detail in the following sections.

4.3.1. Temperature setpoint changes

The setpoint changes were negative for PI, but close to zero or even positive for On/Off (Table 5). This means that the operative temperature stayed most of the time above the desired 21°C even after lowering the air temperature setpoint below 21°C for PI. In both cases, the operative temperature and air temperature fluctuated similarly, yet with an offset. Regarding the On/Off case, the fluctuations were much larger, and the setpoint had to be higher. An example of this behaviour is shown in Figure 17, where line typology corresponds to air temperature setpoint (dotted), air temperature (solid) and operative temperature (dashed).

Figure 17. Air and operative temperature comparison during one January day for PI (P_CP) and On/Off (O_CP) cases. Grey line shows 21°C reference.

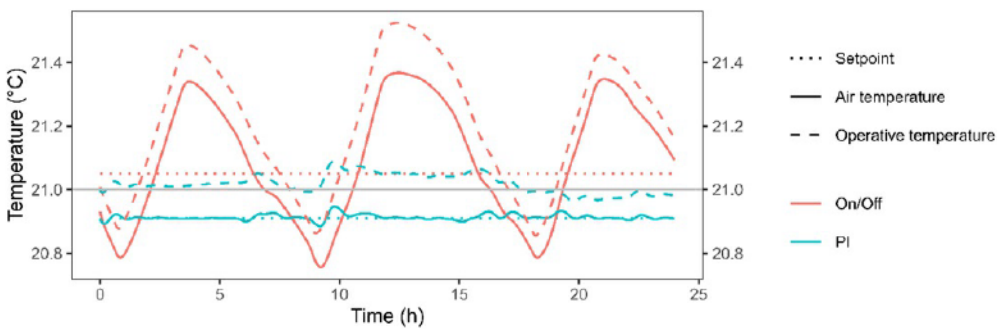

Figure 18 portrays all the shifted operative temperatures by cumulating their occurrence durations. While temperatures in January stayed close to the original setpoint for the whole week, except for some hours, the solar gains in February raised the temperatures. These rose over 24°C and were more than a degree over the setpoint for about 20% of the week. The two extra high temperature cases are the O_0 cases for January and February weeks; the others lie closer together, although the solid (On/Off) lines are relatively higher. This agrees with Table 5, where in all cases except P_WM the temperature fluctuations were clearly smaller for PI than for the corresponding On/Off cases. WM cases are shown in darker colour and thicker lines in Figure 18.

Figure 18. Cumulative operative temperature graphs after setpoint correction for all cases.

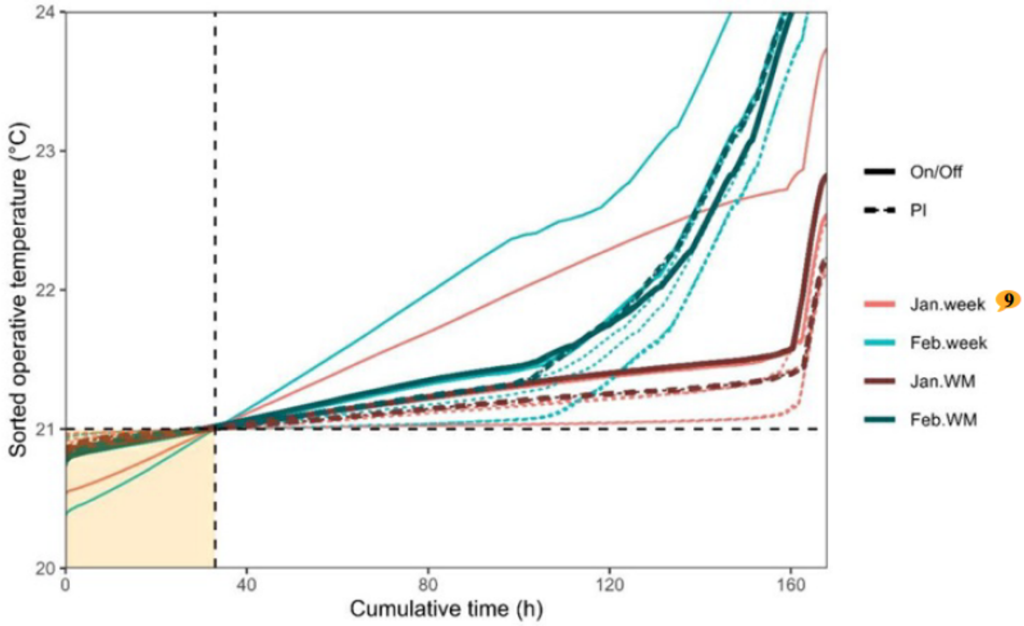

4.3.2. Temperature fluctuations

For On/Off, the source of temperature fluctuations is the dead band (T_{Db}). The setpoint change and MAE of O_0 cases (T_{Db} = 2 K) were much higher than for the rest of the cases (T_{Db} = 0.5 K). While MAE for On/Off in January is mostly around 0.2 K, it was around 0.6 K for the default (O_0) case. Due to symmetric fluctuations around the air temperature setpoint, the MAE is close to 60% of the dead band in all On/Off cases.

The fluctuations for PI were induced by non-optimal parameters as well as modulation. While non-optimal parameters alter the continuous signal, modulation translates it to On/Off-like signal. The theoretical development of control signal for P_WM was described in Figure 8. From simulation outputs, an excerpt was chosen to visualize this development from PI output signal to valve curve output, and it is shown in Figure 19.

Figure 19. Control signal development for P_WM during 4 hours. Outputs from PI (PI), modulation (MC), wax motor (WM), and valve curve (VC) blocks.

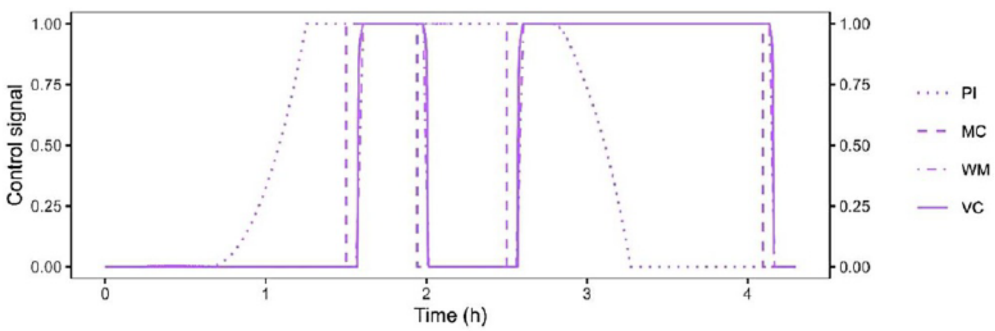

This translation from continuous to binary signal resulted in the PI cases with modulation cases, P_MC and P_WM, having MAEs close to the On/Off cases from 'CP' to 'WM'. The temperature fluctuations for the P_WM and O_WM cases are shown in Figure 20, together with the benchmark cases P_0 and O_0 as well as the improved parameter cases P_CP and O_CP. Significantly higher fluctuations occurred at a greater dead band for On/Off (O_0 case), and the smaller dead band starting from O_CP improved the On/Off control remarkably. Improved PI parameters resulted in an almost ideal control, while modulation and WM delay reintroduced the temperature fluctuations. Altogether, the temperature performance of cases P_0, O_CP, O_WM, and P_WM was similar, and the WM cases could be substituted by simpler control in simulations. The similarity between On/Off and PI occurred as the PI cases did not perform optimally, while the On/Off cases improved significantly from O_0. In this work, the adapted dead band for On/Off was chosen to be 0.5 K. For this to be realized, the room air temperature sensor must be precise, calibrated, and positioned optimally. The room air should also be ideally mixed. Even though the vertical gradient for UFH should be small(Maivel, Ferrantelli, and Kurnitski 2018; Võsa, Ferrantelli, and Kurnitski 2019), realizing one single uniform temperature per zone is clearly still an idealization.

Figure 20. Air temperature fluctuations for detailed cases (O_WM, P_WM) in January, the default cases (O_0, P_0) are shown in comparison as well as the cases with improved parameters (O_CP, P_CP), grey helper lines are at 21 ± 0.25°C.

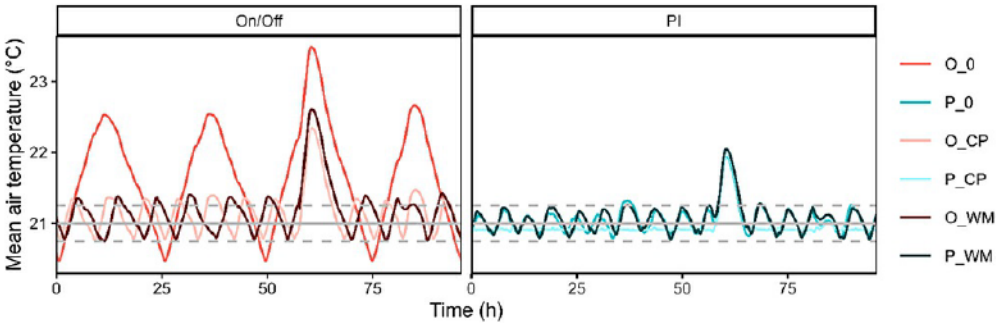

4.3.3. Energy consumption

The energy performance in the given scenarios varied significantly across their levels of detail. Simply modelling the wax motor instead of continuous control (VC to WM case) showed up to 2.5% energy consumption difference in the observed weeks, as Table 5 illustrates. This is consistent with the literature, see e.g. Clauß and Georges(2019) and references quoted therein. Extended to an annual basis, this can be a sizeable effect for energy efficiency.

Although the short delays and the modelling of the valve curve had less influence on the total energy performance, these resulted in different load profiles (see the next section). We found that the choice of parameters for both On/Off and PI, as well as the modelling of modulation in the PI case, had a significant effect. All On/Off cases overestimated the energy consumption compared to the most detailed case (O_WM). For the business-as-usual approach (O_0) the difference was 5.7% for On/Off in the January week and 4.8% in the February week. The business-as-usual PI case P_0 with default parameters and no modulation differs from the other simple PI cases (P_CP, P_D, P_VC – optimal parameters, no modulation). Yet, its energy consumption was like that of the modulation cases P_MC and P_WM with optimal parameters and modulation. P_0 overestimated the energy consumption by 0.1% in the January week and 0.7% in February compared to P_WM. However, all the other PI cases underestimated the energy consumption compared to P_WM.

As in most cases, a lower energy consumption was achieved thanks to smaller temperature fluctuations, which enabled a lower temperature setpoint. The step from '0' to 'CP', with reduction of energy use by using improved PI parameters, was over 3.4 percentage points in the February week. The reduction in temperature fluctuation from optimal PI parameters was cancelled out by an increase in fluctuations, which was caused by the conversion of the continuous PI output to binary values, so from P_VC to P_MC, and by wax motor delay, from P_MC to P_WM. The step from '0' to 'CP' was higher than the 2.5% increase from 'VC' to 'WM', adding modulation and WM, in the February week. This highlights the importance of optimal PI parameters. However, the parameters that were optimized in the business-as-usual situation did not perform optimally together with a modulation approach. The optimized parameters for continuous PI control (without modulation) can thus be potentially used for 0–10 V actuators, while the coupling of modulation with parameters' optimization should be further researched. The PI parameters that were specifically adapted to the applied modulation could potentially improve the performance (Appendix D).

In most occurrences anyway, the PI cases consumed less heating energy than the corresponding On/Off cases. While for On/Off and PI business-as-usual, the PI was almost 6% more efficient for both weeks (2.41 vs. 2.55 and 2.31 vs. 2.42), there was practically no difference in the WM cases. The difference between O_WM and P_WM is generally smaller than the rest, holding at 0.2% in January and 2.1% in February. For the 'CP' through 'VC' cases it approached 2% in January and 5% in February. Therefore, substituting the PI with WM modelling with On/Off as suggested for temperature fluctuations in Section 4.3.2 would not provide the same energy performance. The smallest difference was to O_VC and to P_0.

4.3.4. Load dynamics

All the business-as-usual cases overestimated the energy consumption, leaving the results on the safe side regarding system design. However, it was clear that the volume flows in the circuit are different between the business-as-usual and the WM cases. Both overestimation of energy consumption and inaccurate mass flows could be non-conservative for other applications such as grid balancing, structural thermal storage, etc.

To better understand the development of energy consumption, Figure 21 displays on separate rows the mass flows (row a), water return temperatures (row b), and floor surface heat flux (row c) as cumulative for the January week. The outdoor temperature-dependent supply temperatures were the same for all scenarios and are portrayed as dashed lines in charts 1b and 2b.

Figure 21. Cumulative performance in the January week.

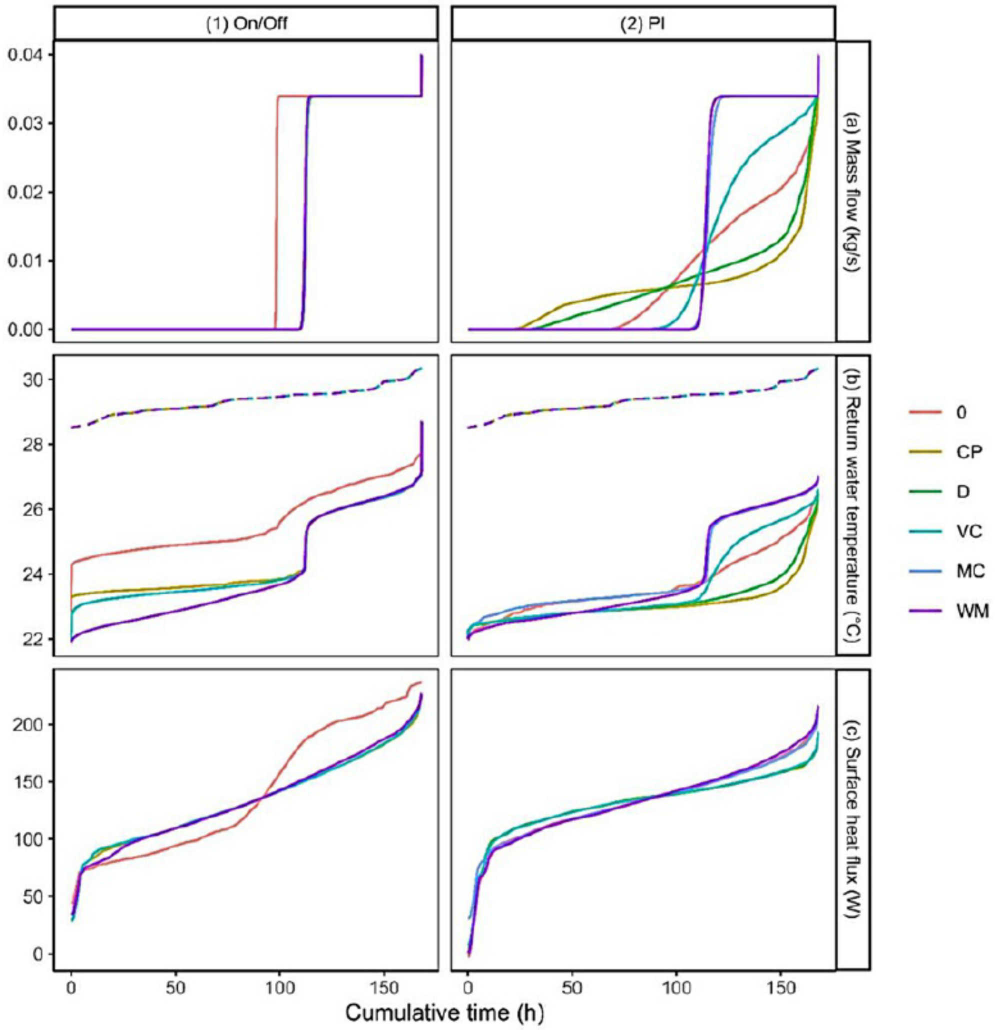

For the On/Off scenarios, O_0 stands out from the rest. For PI, the distribution of mass flows, return temperatures as well as heating loads vary between all the cases, including 'CP', 'D', and 'VC'. These otherwise performed similarly, differing by no more than 0.01 K in setpoint, 0.015 K in MAE(T), and by 0.5 percentage points (0.01 kWh/m²/week) in energy consumption during one given week. This means that adding a 2-min delay to the input signal and correcting the valve curve did not have a significant effect on the air temperature and energy performance. However, it changed the mass flow dynamics. P_MC and P_WM had mass flows like those of the binary On/Off cases, while the 'CP' and 'D' cases had mass flows mostly at the 25% level. P_0 and P_VC were between the two extremes, with a close to linear flow.

Adding a WM had almost no influence in January compared to the control that was simpler by one step, either O_VC or P_MC. However, the cumulative graphs in Figure 21 show that the return temperatures for the WM scenarios were lower. This would refer to a different timing of the heating periods in relation to outdoor temperatures. Adding the WM in February, the energy consumption decreased for On/Off and increased for PI. For On/Off, the additional delay from the WM reduced the MAE and energy consumption. This could be due to the combination of delay and solar gains, as the two charts on the left side of Figure 22 show. The delay enabled to omit one heating cycle when solar gains emerged, keeping lower solar peak temperatures. For PI, the additional delay generated higher temperature fluctuations and, due to the higher induced setpoint, this increased the consumption (see the two charts on the right in Figure 22).

Figure 22. Control and temperature during a day in February, hours from midnight, grey line showing the shifted setpoint.

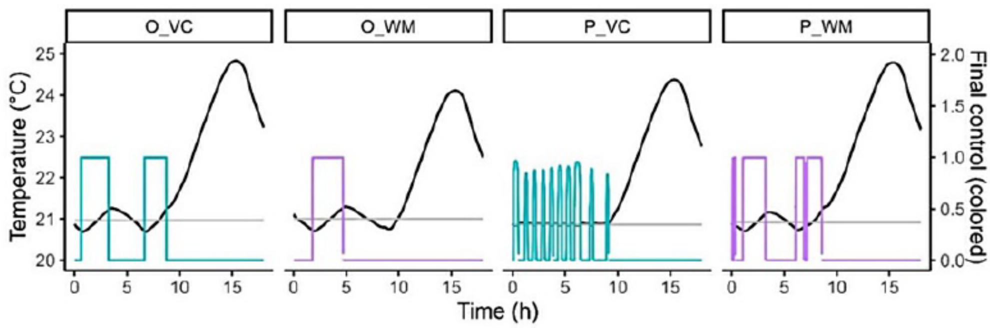

5. Conclusions[6]

In this paper, we have attempted at shedding light on two aspects of UFH control modelling by

- analysing how a stepwise increase in the modelling detail can affect its performance, regarding both temperature fluctuations and energy consumption,
- proposing an empirical wax motor model, calibrating it with extensive experimental results, and implementing as well as testing it with simulations.

To such aim, an experimentally based empirical model of thermo-electric actuators, or wax motors used in HVAC control was here developed. The experimental aspect was addressed into detail, first by measuring the linear displacement of the attached valve's piston without the rest of the system. Based on these measurements, we defined an empirical model consisting of four sub-models of linear segments that estimated the characteristic times. The final model resulted in an average MAE of normalized linear displacement that stayed below 10%.

The volume flows were then measured within one circuit of an UFH system with a predefined control signal that was applied to the wax motor. Based on the volume flow measurements, the valve curve was calibrated, and the models were finally implemented in the IDA ICE simulation software, for quantifying the effect of the models on BPS results.

Referring to the research questions that were formulated in the Introduction, they can now be answered as follows:

1 How can we characterize the wax actuators for HVAC in an applicable way?

a The developed empirical wax motor model consists of dead time, rise time, hold time, and fall time, which depend on undercooling or overheating times. The dead time was up to 4 min, the rise time up to 3 min, the hold time up to 2.5 or 4 min depending on the motor product. As an exception, the fall time was constant for one product, either 2 or 3 min. Adapting the developed models to new products does not need extensive modelling nor expensive measurements.

2 How much time does the valve opening with wax motors take? Can it be managed within 5 min, so that it would match the limit imposed by the frequency market for energy grids?

a After longer undercooling times, the wax heated up slowly, showing that the full activation time, i.e. the valve opening time, can be larger than 5 min. However, the maximum FAT did not exceed 7 min. Quick-opening valve curves, together with a low valve authority, ensured that nearly maximal flow rates were reached with 50% valve openness. If a shorter FAT is needed, the wax actuators should be continuously kept on standby, thus applying short heating cycles.

3 How are temperature control accuracy and energy performance affected by the control strategy?

a Modelling the control with the empirical wax motor model, including modulation for PI, valve curves, signal delays and realistic parameter values is important for some applications. Compared to including all these options, a business-as-usual BPS overestimated the energy consumption by 5% for On/Off and less than 1% for PI. While for On/Off the temperature fluctuations were reduced by a smaller dead band, for PI these were increased due to modulation. The temperature variations were thus critically affecting the energy balance.

4 How do wax motor and modulation effects compare to performance differences from other modelling simplifications?

a Changing control parameters and adding modulation resulted in the largest changes regarding all the steps taken for detailing the control modelling. The control parameters changed energy consumption by about 2%–5% and adding modulation by 2%–3%. Adding a wax motor when the heating signal was already binary changed the result by less than 1%.

As a practical consideration, it was found that the business-as-usual PI control did not reflect the actual mass flows in the system. The actual behaviour is similar to that of the On/Off behaviour, so the PI simulations could be substituted by On/Off simulations with a small dead band, and an actual valve curve but without the wax motor. However, the temperature setpoint in the simulations had to be set higher than for the PI by at least 0.1 K, to ensure the same energy performance.

The work has some limitations, which should be further analysed in future studies:

- The study can be extended on several aspects, for instance by implementing a physical model for 0–10 V wax actuators, which could also model profiles where the motor does not completely open/close the valve during each period. Experiments to determine properties of the spring, the wax, and the motor cover should be carried out accordingly. The piston movement inside the manifold should be measured as well.
- Also, the implemented empirical model currently uses very small timesteps, making it time-and resource-consuming when used for simulations involving longer time spans. Speeding up the model with a carefully performance-optimized implementation would enable simulating annual energy consumption differences.
- Finally, as the parameters that were optimized in the business-as-usual situation might not work optimally together with a modulation approach, the coupling of modulation with the parameters' optimization should be further researched.

Disclosure statement

No potential conflict of interest was reported by the author(s **[Q6]**).

ORCID

Tuule Mall Parts http://orcid.org/0000-0002-2170-9575

Data availability statement

The data that support the findings of this study are available from the corresponding author, T.M.P, upon reasonable request.

References

~~Akaike, H. 1974. "A New Look at the Statistical Model Identification." *IEEE Transactions on Automatic Control* 19 (6): 716–723~~**[Q7]**~~. doi:10.1109/TAC.1974.1100705.~~

Artelys. 2017. *METIS Technical Note T6 – METIS Power System Module*. Brussels: European Commission.

Beijing MUYY Technologies Co., Ltd. 2023. "Electric Thermal Actuator – TRV Head," [Online]. Accessed 7 February 2023. https://www.muyytec.com/portfolio-items/electric-thermal-actuator/.

Bienvenido-Huertas, D., C. Rubio-Bellido, D. Marín-García, and J. Canivell. 2021. "Influence of the Representative Concentration Pathways (RCP) Scenarios on the Bioclimatic Design Strategies of the Built Environment." *Sustainable Cities and Society* 72: 103042. doi:10.1016/j.scs.2021.103042.

Boßmann, T., and I. Staffell. 2015. "The Shape of Future Electricity Demand: Exploring Load Curves in 2050s Germany and Britain." *Energy* 90 (2): 1317–1333. doi:10.1016/j.energy.2015.06.082.

Burt, S., and M. de Podesta. 2020. "Response Times of Meteorological Air Temperature Sensors." *Quarterly Journal of the Royal Meteorological Society* 146: 2789–2800. doi:10.1002/qj.3817.

CEN. 2008. *EN 15377-1:2008*. Bruxelles: European Committee for Standardization.

CEN. 2019. *EN 16798-2:2019*. Bruxelles: European Committee for Standardization.

Clauß, J., and L. Georges. 2019. "Model Complexity of Heat Pump Systems to Investigate the Building Energy Flexibility and Guidelines for Model Implementation." *Applied Energy* 255: 113847. doi:10.1016/j.apenergy.2019.113847.

Danfoss A/S. 2017. *Actuator ABNM A5 0-10V Proportional For Use with RA2000 Valves*. Nordborg: Danfoss A/S.

Elnaklah, R., I. Walker, and S. Natarajan. 2021. "Moving to a Green Building: Indoor Environment Quality, Thermal Comfort and Health." *Building and Environment* 121: 107592. doi:10.1016/j.buildenv.2021.107592.

EQUA AB. 2020. *IDA Indoor Climate and Energy (IDA ICE, Version 4.8 SP2, Expert edition)*. Solna: EQUA AB.

Fingrid Oyj. 2022. "Reserve Products and Reserve Market Places," Fingrid Oyj. [Online]. Accessed 19 May 2022. https://www.fingrid.fi/globalassets/dokumentit/en/electricity-market/reserves/reserve-products-and-reserve-market-places.pdf.

Goia, F., G. Chaudhary, and S. Fantucci. 2018. "Modelling and Experimental Validation of an Algorithm for Simulation of Hysteresis Effects in Phase Change Materials for Building Components." *Energy and Buildings* 174: 54–67. doi:10.1016/j.enbuild.2018.06.001.

HBK. 2021. *QUANTUM MX840A Universal Amplifier – Data Sheet*. Halifax: HBK.

HBK. 2022. *QUANTUM CX22B-W/CX22B – Data Sheet*. Egham: HBK.

HBM Finland. 2022. "WI: Inductive Displacement Transducer (Miniature Probe)," HBM Finland. [Online]. Accessed 19 May 2022. https://www.hbm.com/en/3060/wi-inductive-displacement-transducer-miniature-probe/.

Johnson Controls LTD. 2020. *Valve and Actuator Manual*. Cork: Johnson Controls.

Kalamees, T., and J. Kurnitski. 2006. "Estonian Test Reference Year for Energy Calculations." *Proceedings of the Estonian Academy of Sciences. Engineering* 12 (1): 40–58. doi:10.3176/eng.2006.1.04.

Klimeš, L., P. Charvát, and M. Ostrý. 2019. "Thermally Activated Wall Panels with Microencapsulated PCM: Comparison of 1D and 3D Models." *Journal of Building Performance Simulation* 12 (4): 404–419. doi:10.1080/19401493.2018.1543350

Kull, T. M., M. Thalfeldt, and J. Kurnitski. 2019a. "Estimating Time Constants for Underfloor Heating Control." *Journal of Physics: Conference Series* 1343 (1): 012121. doi:10.1088/1742-6596/1343/1/012121.

Kull, T. M., M. Thalfeldt, and J. Kurnitski. 2019b. "Optimal PI Control Parameters for Accurate Underfloor Heating Temperature Control." *E3S Web of Conferences* 111: 01081. doi:10.1051/e3sconf/201911101081.

Kull, T. M., M. Thalfeldt, and J. Kurnitski. 2020. "PI Parameter Influence on Underfloor Heating Energy Consumption and Setpoint Tracking in nZEBs." *Energies* 13 (8): 2068. doi:10.3390/en13082068.

Kull, T. M., M. Thalfeldt, and J. Kurnitski. 2021. "Modelling of Wax Actuators in Underfloor Heating Manifolds." In Cold Climate HVAC &

Energy 2021, Tallinn, Estonia.

Kumar, P. 2017. "Valve Trim Design Using Control Valve Performer," 21 October 2017. [Online]. Accessed 9 May 2022. Available: https://www.simulationhub.com/blog/valve-trim-design-using-control-valve-performer.

Le Dréau, J., and P. Heiselberg. 2016. "Energy Flexibility of Residential Buildings Using Short Term Heat Storage in the Thermal Mass." *Energy* 111: 991–1002. doi:10.1016/j.energy.2016.05.076.

Li, Y., N. Nord, H. Wu, Z. Yu, and G. Huang. 2020. "A Study on the Integration of Air-Source Heat Pumps, Solar Collectors, and PCM Tanks for Outdoor Swimming Pools for Winter Application in Subtropical Climates." *Journal of Building Performance Simulation* 13 (6): 662–683. doi:10.1080/19401493.2020.1813198.

Lindab, A. B. 2021. *Lindab Actuators - Actuator 24 V*. Båstad: Lindab AB.

Lindahl, M. 2020. *Grid Flexible Control of Heat Pumps*. HPT - Heat Pumping Technologies.

Maivel, M., A. Ferrantelli, and J. Kurnitski. 2018. "Experimental Determination of Radiator, Underfloor and Air Heating Emission Losses due to Stratification and Operative Temperature Variations." *Energy and Buildings* 166: 220–228. doi:10.1016/j.enbuild.2018.01.061.

Majandus-ja taristuminister. 2015. "Hoone energiatõhususe arvutamise metoodika," 1 July 2015. [Online]. Accessed 13 May 2022. https://www.riigiteataja.ee/akt/109062015021?leiaKehtiv.

Okur, Ö, P. Heijnen, and Z. Lukszo. 2021. "Aggregator's Business Models in Residential and Service Sectors: A Review of Operational and Financial Aspects." *Renewable and Sustainable Energy Reviews* 139: 110702. doi:10.1016/j.rser.2020.110702.

Pedersen, T. H., R. E. Hedegaard, and S. Petersen. 2017. "Space Heating Demand Response Potential of Retrofitted Residential Apartment Blocks." *Energy and Buildings* 141: 158–166. doi:10.1016/j.enbuild.2017.02.035.

Petitjean, R. 1994. *Total Hydronic Balancing: A Handbook for Design and Troubleshooting of Hydronic HVAC Systems*. Ljung: Tour & Andersson AB.

R Core Team. 2020. *R: A Language and Environment for Statistical Computing*. Vienna: R Foundation for Statistical Computing.

Reynders, G., J. Diriken, and D. Saelens. 2017. "Generic Characterization Method for Energy Flexibility: Applied to Structural Thermal Storage in Residential Buildings." *Applied Energy* 198: 192–202. doi:10.1016/j.apenergy.2017.04.061.

Rizzello, G., D. Naso, and S. Seelecke. 2019. "Hysteresis Modeling in Thermal Shape Memory Alloy Wire Actuators: An Irreversible Port-Hamiltonian Approach." In *2019 IEEE 58th Conference on Decision and Control (CDC)*, 7937–7943.

Rogelj, J., et al. 2018. "Scenarios Towards Limiting Global Mean Temperature Increase Below 1.5 °C." *Nature Climate Change* 8 (4): 325–332. doi:10.1038/s41558-018-0091-3.

Sensus Inc. 2021. *PolluStat E - Data Sheet*. Morrisville: Sensus Inc.

Siemens, A. G. 2021. *LOGO! 24CE Logic Module, 6ED1052-1CC08-0BA1*. Munich: Siemens AG.

The Underfloor Heating Site. 2023. "Reliance Manifold Thermoelectric Head." [Online]. Accessed 7 February 2023. https://theunderfloorheatingsite.co.uk/shop/water-under-floor-heating/accessories/actuators/manifold-thermoelectric-head/.

Ventilation Control Products Sweden AB. 2022. "Thermoelectric Valve Actuators and Valve Adaptors for Different Valve Brands," 2011-2022. [Online]. Accessed 23 October 2022. http://www.ventilationcontrolproducts.net/actuators-and-valve-adaptors.

Vernatherm. 2023. "Thermal Actuators (Wax Motors)." [Online]. Accessed 7 February 2023. Available: https://www.vernatherm.com/thermal_actuators.html.

Võsa, K.-V., A. Ferrantelli, and J. Kurnitski. 2019. "Experimental Study of Radiator, Underfloor, Ceiling and Air Heater Systems Heat Emission Performance in TUT nZEB Test Facility." *E3S Web of Conferences* 111: 04005. doi:10.1051/e3sconf/201911104005.

Wen, J., and T. F. Smith. 2001. "Effect of Thermostat Time Constant on Temperature Control and Energy Consumption." SIcon/01. Sensors for Industry Conference. Proceedings of the First ISA/IEEE. Sensors for Industry Conference (Cat. No.01EX459), 252–257.

Wetter, M.. 2009. "A Modelica-based Model Library for Building Energy and Control Systems". Lawrence Berkeley National Laboratory. 11th International Building Performance Simulation Association Conference - Building Simulation '09. Glasgow, Scotland. July 27-30, 2009. **[Q8]**

Wolisz, H., T. M. Kull, D. Müller, and J. Kurnitski. 2020. "Self-learning Model Predictive Control for Dynamic Activation of Structural Thermal Mass in Residential Buildings." *Energy And Buildings* 207: 109542. doi:10.1016/j.enbuild.2019.109542.

Wolisz, H., C. Punkenburg, R. Streblow, and D. Müller. 2016. "Feasibility and Potential of Thermal Demand Side Management in Residential Buildings Considering Different Developments in the German Energy Market." *Energy Conversion and Management* 107: 86–95. doi:10.1016/j.enconman.2015.06.059.

Zhang, L., N. Good, and P. Mancarella. 2019. "Building-to-Grid Flexibility: Modelling and Assessment Metrics for Residential Demand Response from Heat Pump Aggregations." *Applied Energy* 233–234: 709–723. doi:10.1016/j.apenergy.2018.10.058.

Appendices

A. Measured actuators, heating profiles, and error estimates

Table A1. The error estimations for all profiles.

Combination	Producer	Motor specimen	Valve included?	Heating profiles measured (signal On-Off)	Duration (min)	MAE	RMSE
A1	A	1	no	15 min–45 min	515	0.014	0.042
A1	A	1	no	15 min–15 min	362	0.018	0.047
A1	A	1	no	5 min–5 min	454	0.058	0.089
A1v	A	1	yes	15 min–15 min	2774	0.011	0.019
B1	B	1	no	15 min–45 min	1241	0.023	0.047
B1	B	1	no	30 min–30 min	720	0.020	0.037
B1	B	1	no	10 min–10 min	646	0.045	0.097
B1	B	1	no	18 min–6 min	711	0.033	0.050
B1	B	1	no	15 min–15 min	1049	0.048	0.079
B1	B	1	no	3 min–3 min	141	0.098	0.122
B2	B	2	no	15 min–15 min	1110	0.028	0.048
B1v	B	1	yes	15 min–15 min	118	0.061	0.153
B2v	B	2	yes	15 min–15 min	1090	0.025	0.042
B2v	B	2	yes	15 min–45 min	1486	0.019	0.036
B3v	B	3	yes	15 min–15 min	144	0.030	0.056
B4v	B	4	yes	15 min–15 min	136	0.058	0.106
B4v	B	4	yes	random 5 to 15 min	482	0.086	0.148
B4v	B	4	yes	15 min–45 min	416	0.043	0.090

B. Heating curve for UFH supply water temperature in simulations

Figure B1. Heating temperature curve used in simulations.

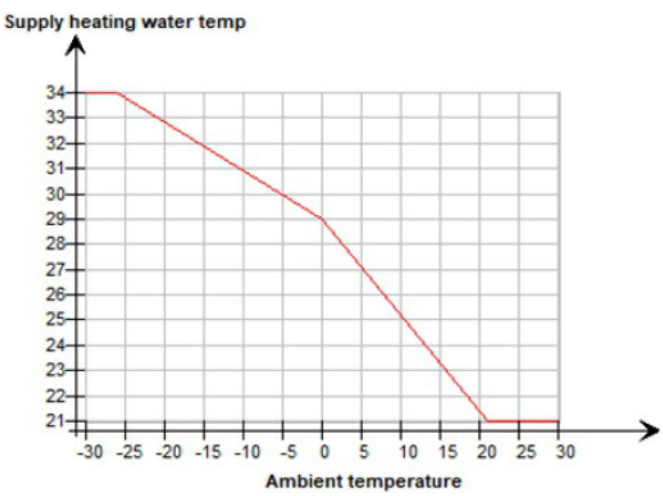

Table C1. The process of fitting the empirical models to the characteristic times estimated from the measurements.

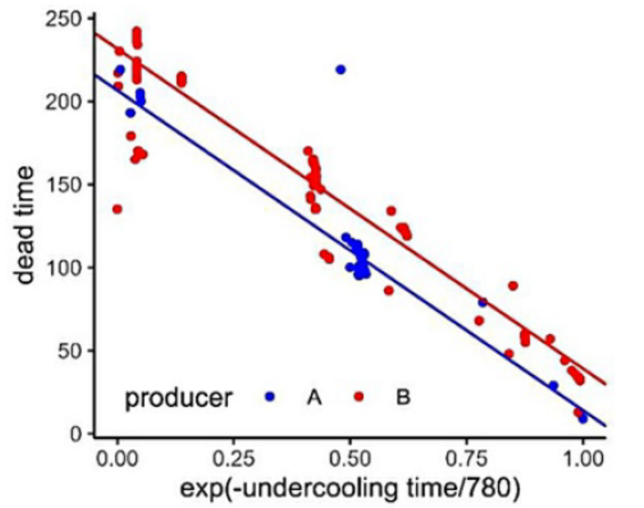

The estimated dead times had a clear dependence on the undercooling time of the previous period, therefore $t_{dead,i} = f(t_{uc,i-1})$. The negative exponent model was fitted as given in Equation (1). The time constant value $\tau = 780$ s had the highest correlation, with R-squared between the negative exponent and the dead time equalling 0.885. However, the linear model resulted in maximum residuals of over 1.5min. To improve the performance, a linear multi-level model was tested and chosen for separate products, which constrained the residuals to maximum 10 s. In the figure, blue is the model for product A and red for the product B.

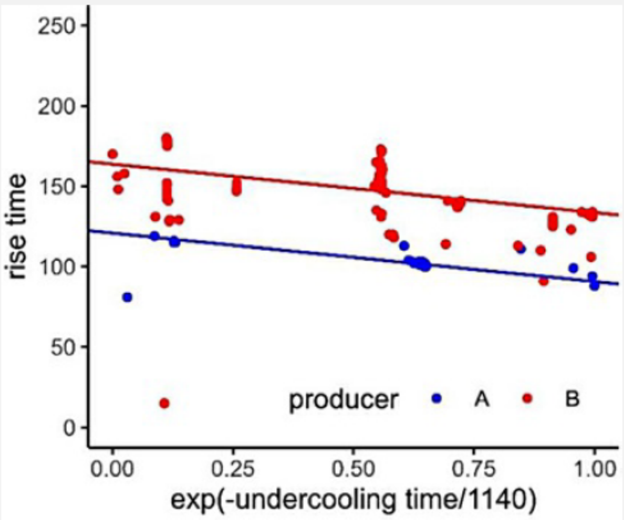

The rise times varied between 100 s and 180 s and it was therefore not constant as expected. The null hypothesis of rise time depending on room temperature was not confirmed as the ambient temperature varied in a very small range during the measurements. Instead, there was a slight dependence on the undercooling time's negative exponent similarly to the dead time. Therefore, $t_{rise,i} = f(t_{uc,i-1})$ where the most suitable τ was 1140 s. The parameter k was small but clearly significant ($p < .001$). The residuals were over two minutes, so instead, a motor-specific solution was again identified using multi-level modelling.

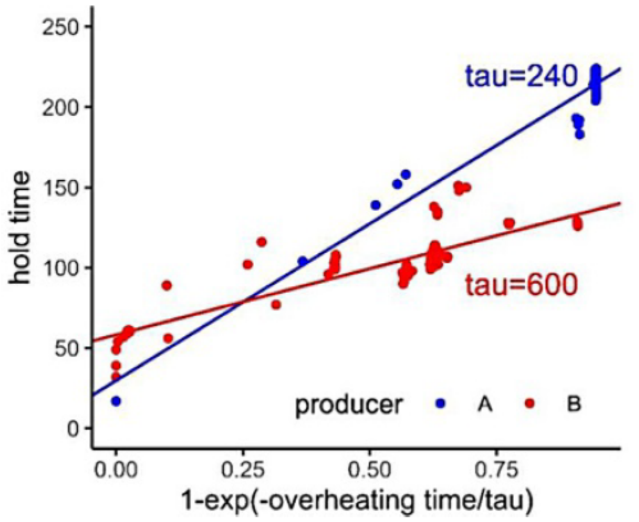

The hold time did depend on the overheating time, as expected in Equation (2). However, the dependence was not significant. As the hold time could be quite different for the motors, as Figure 11 shows. Thus, a producer-separated model was generated. As the intercept was insignificant for lme, separate linear models were fitted. Moreover, as in this case there is no reason to assume the same time constants and parameters, we searched for separate τ values. These resulted to be $\tau = 240$ s for product A and $\tau = 600$ s for product B.

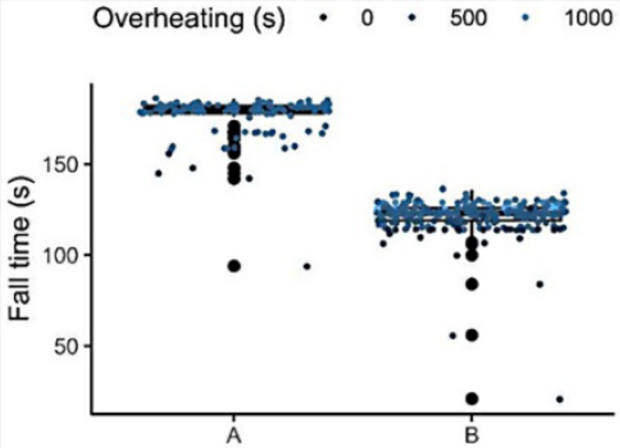

The fall time was constant for a product, as the standard deviation was around 10 s. No room temperature dependence was seen in the data. In the figure, the order of magnitude of the overheating time is shown in three colours for the two products.

D. PI parameters optimized for continuous and modulated output

Figure D1. The cumulative temperature graphs for P_WM case (18/2300) and the same case with PI parameters adapted for the modulation (300/3000).

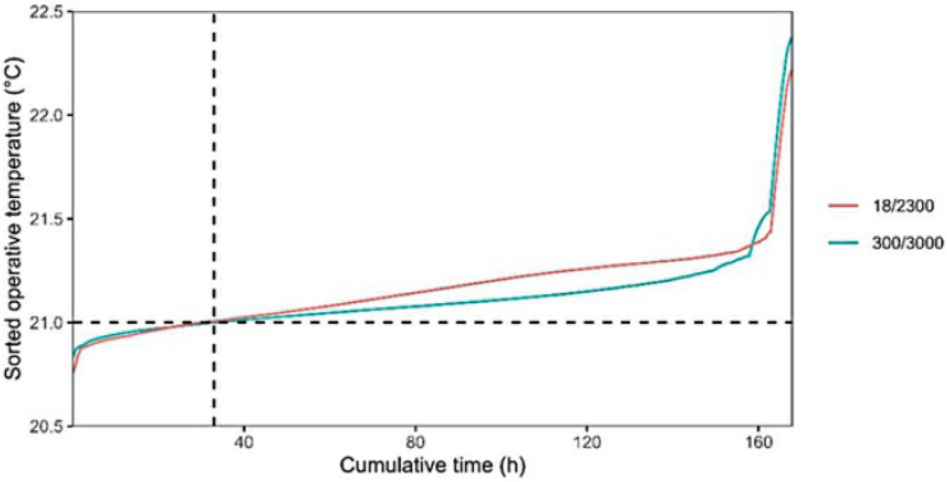

Attachment Files

1 **Figure4.png** :

2 **Figure18.jpg** :

3 **Figure19.jpg** :

4 **Figure21.jpg** :

5 **Figure22.jpg** :